Фазовые переходы в жидкостях и стеклах при высоких давлениях

Фазовые превращения в кристаллах

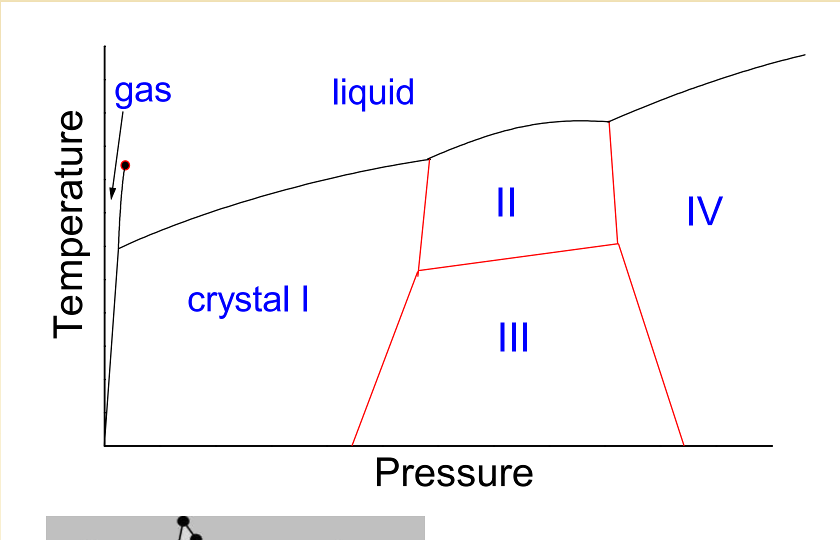

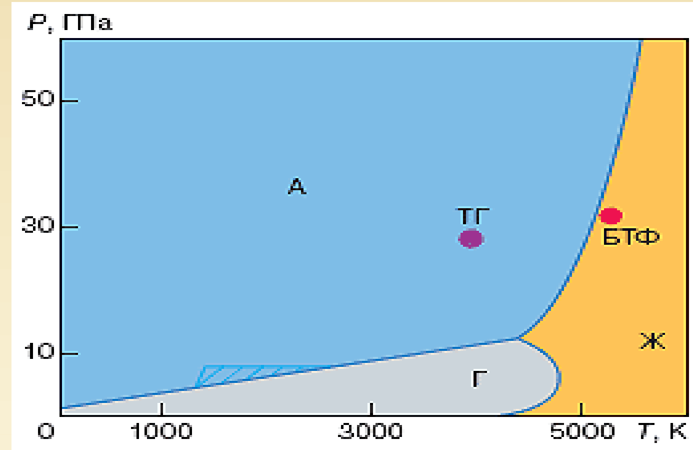

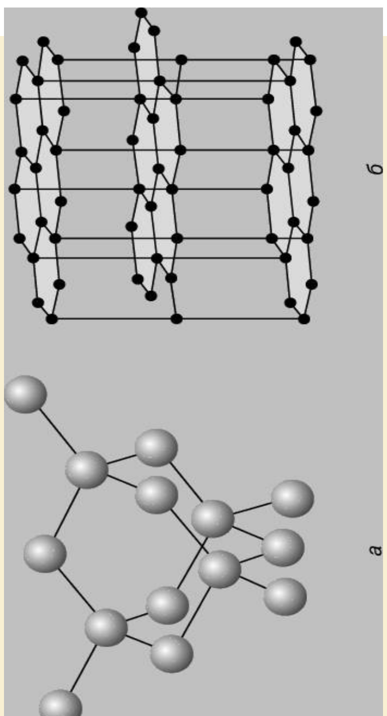

P,T- диаграмма льда

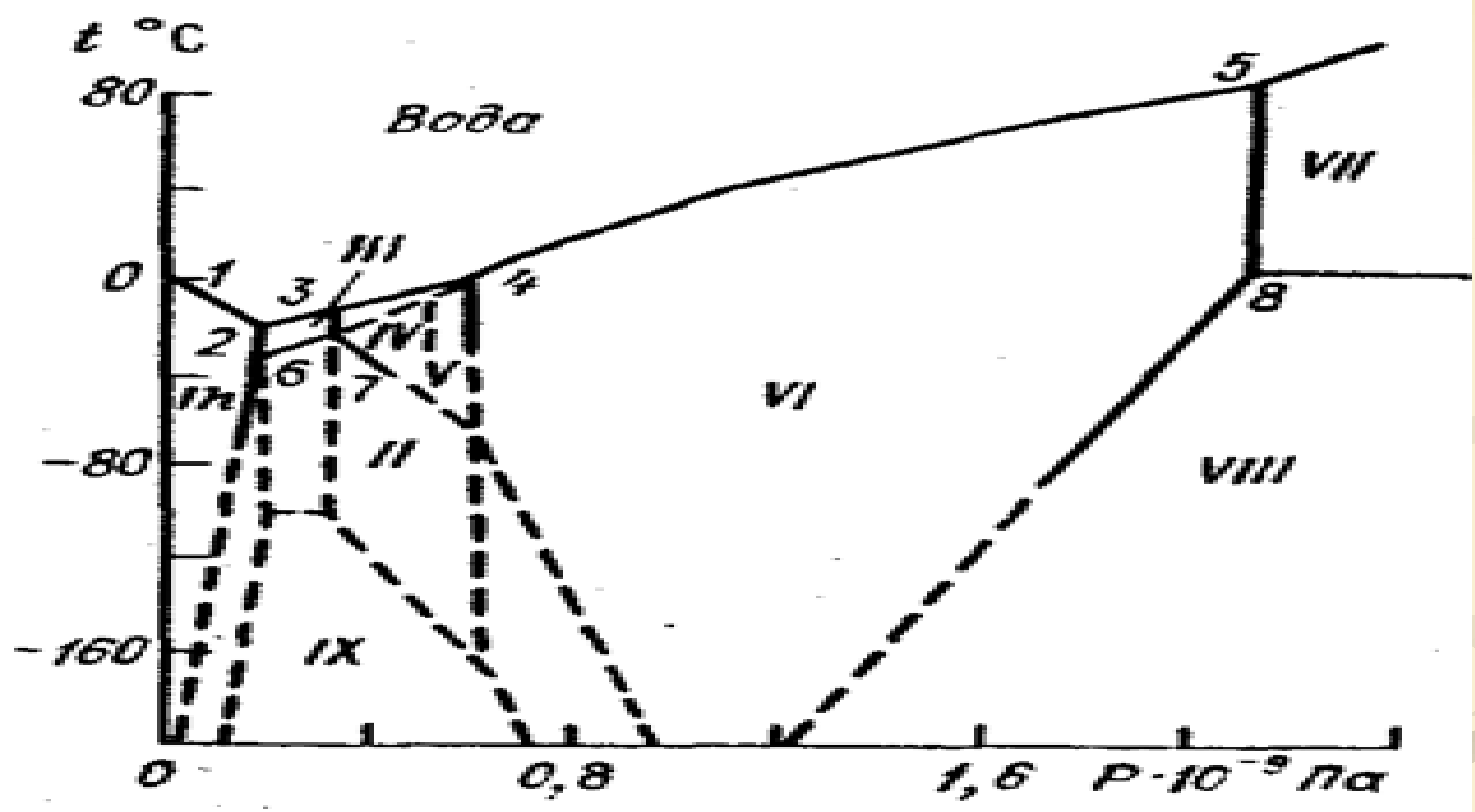

Проблема резких и размытых превращений в жидкостях и стеклах

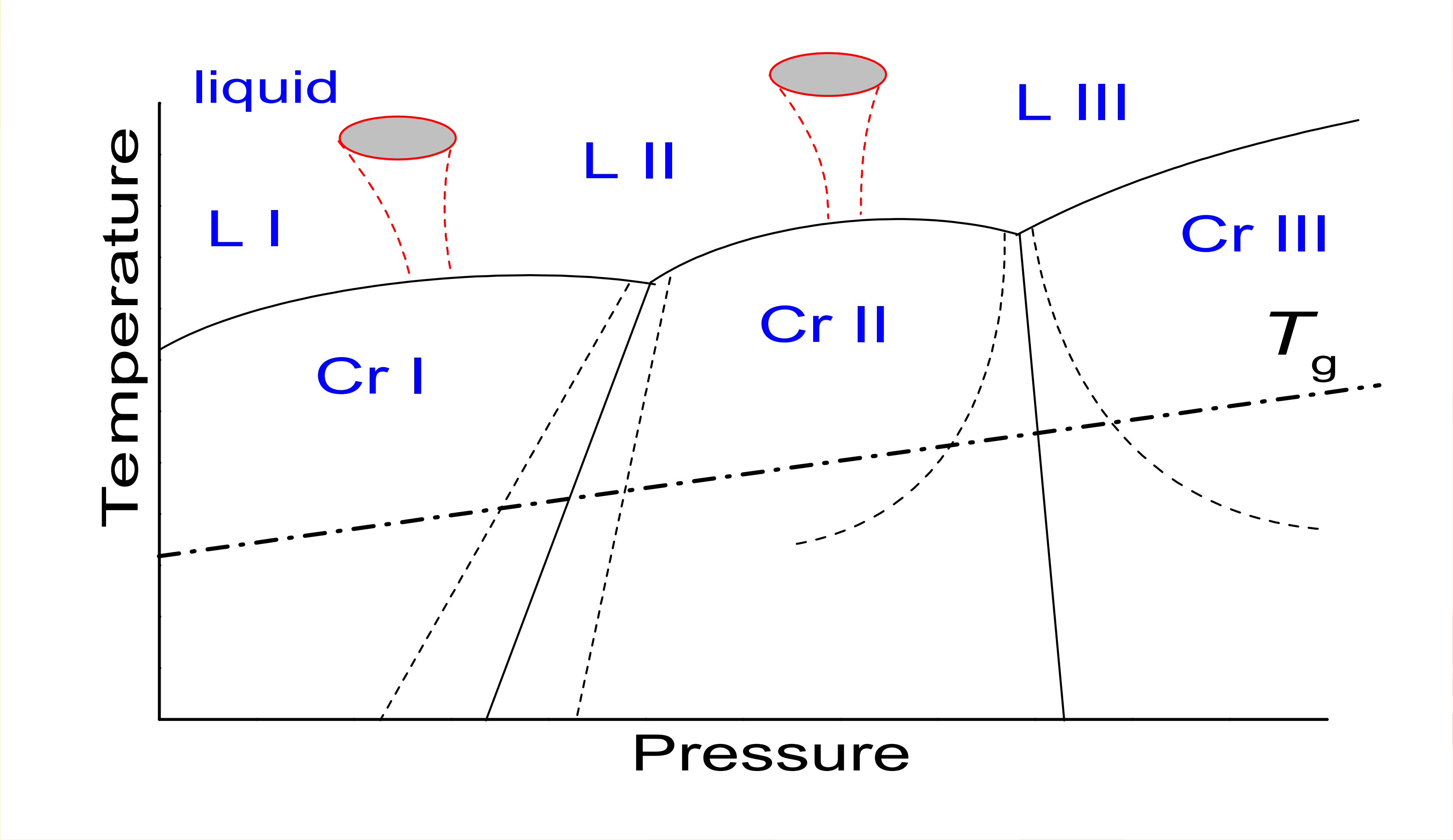

Превращения в элементарных расплавах: Se переход полупроводник-металл в расплаве

Selenium

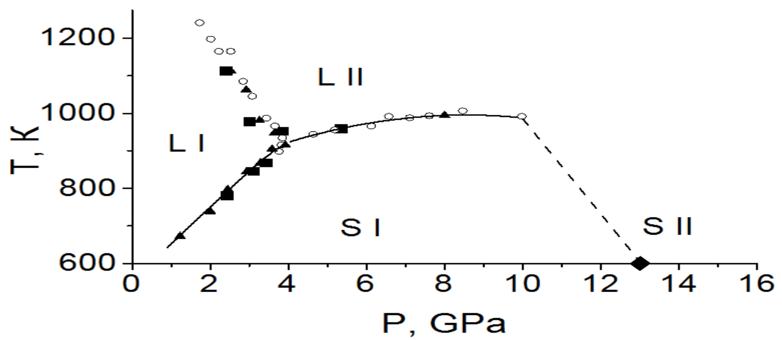

First example of sharp changes of V, S, ρ

ΔP, ΔT ~ 3 kbar, 30 K
at high temperatures: ΔP, ΔT ~ 10 kbar , 200 K

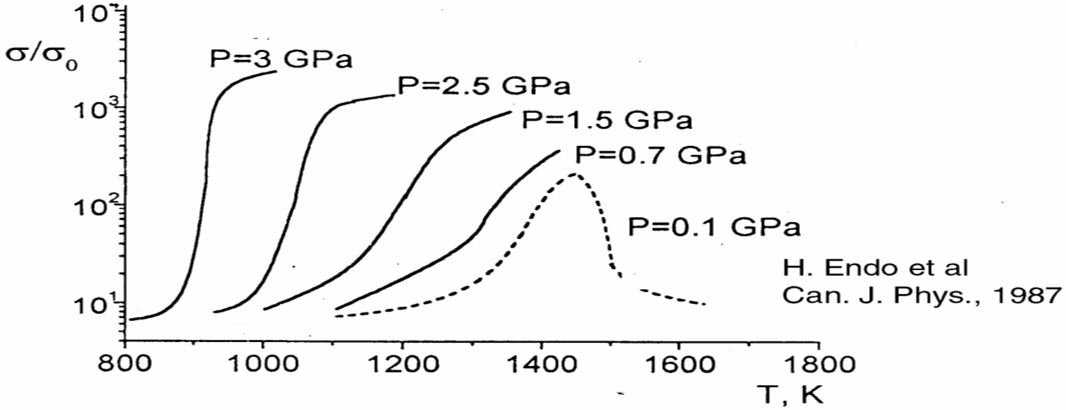

JETP Lett, 50 (1989)

Превращения в элементарных расплавах: Se
переход полупроводник-металл в расплаве

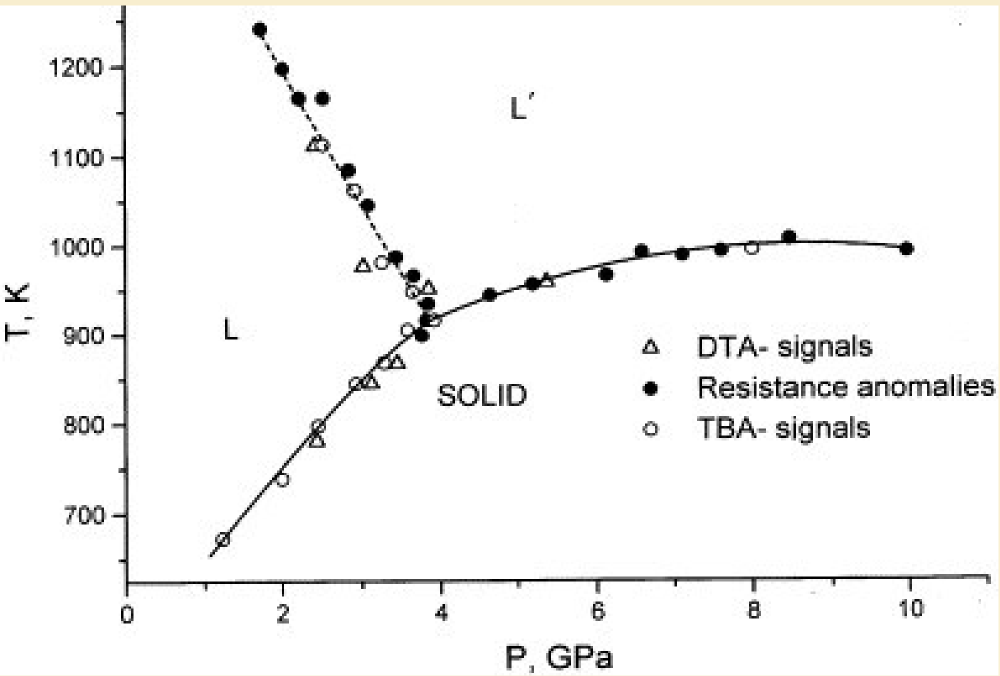

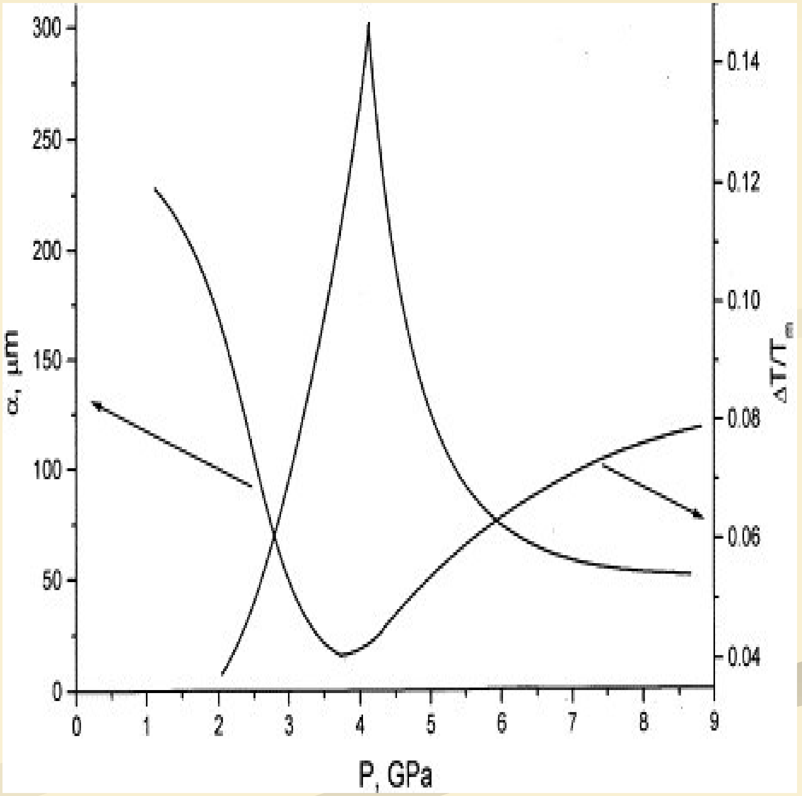

Вязкость расплава Se под давлением

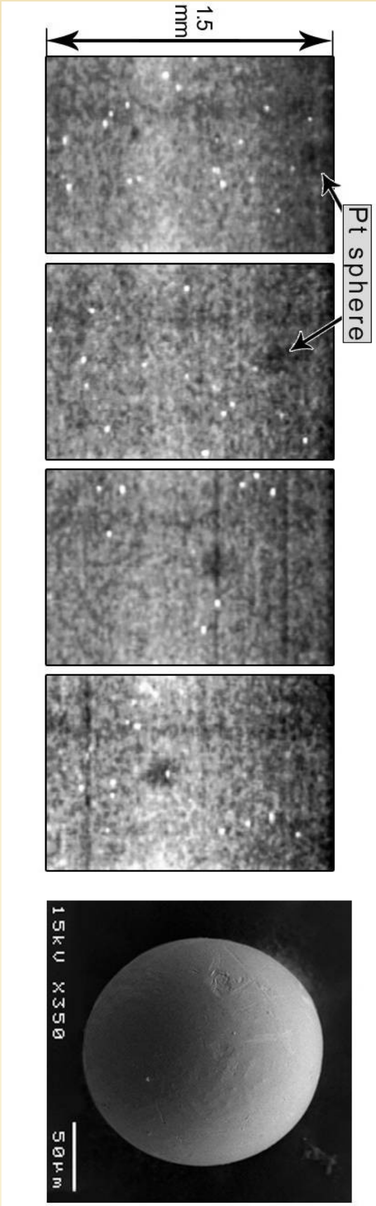

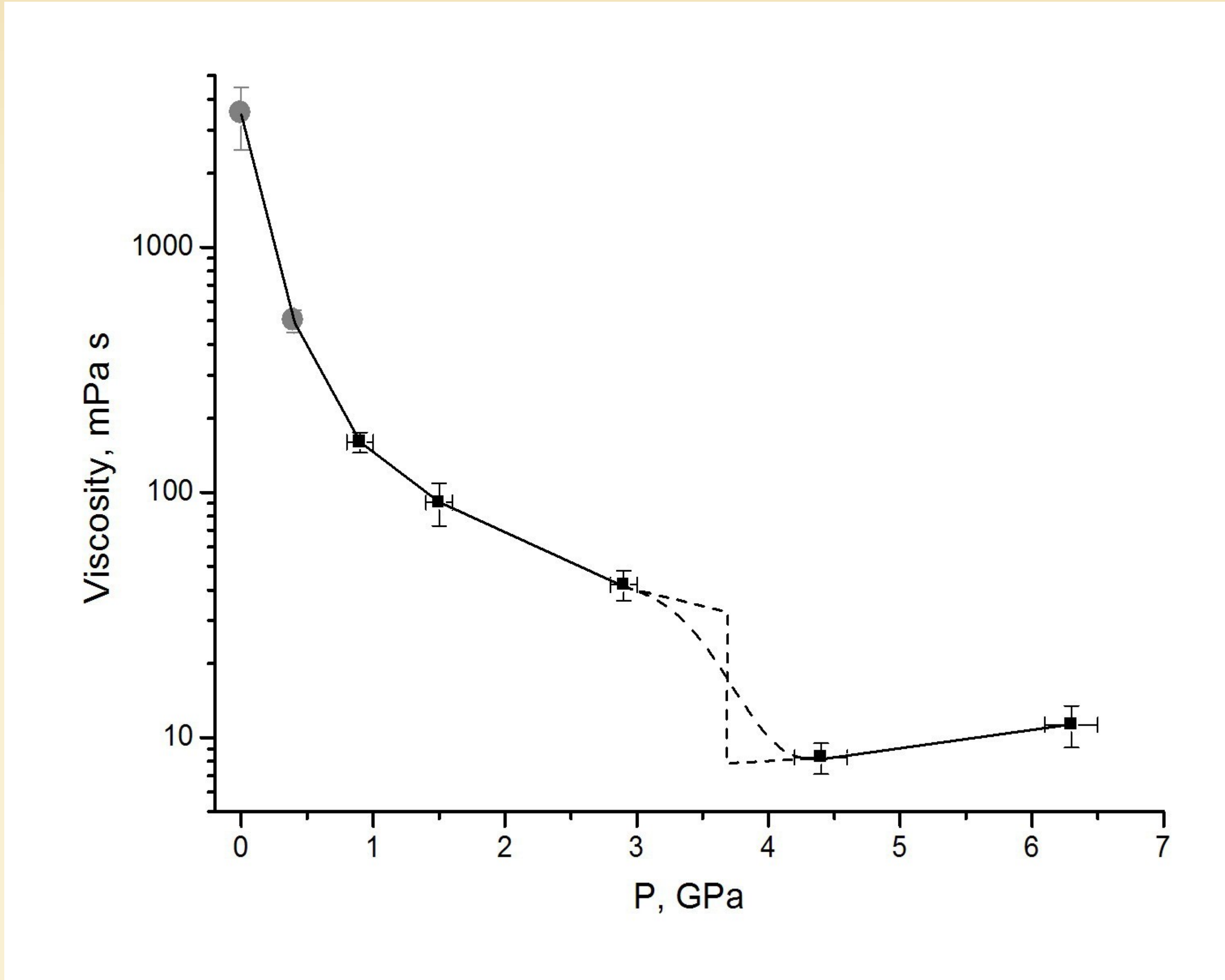

Фазовый переход первого рода в жидком фосфоре

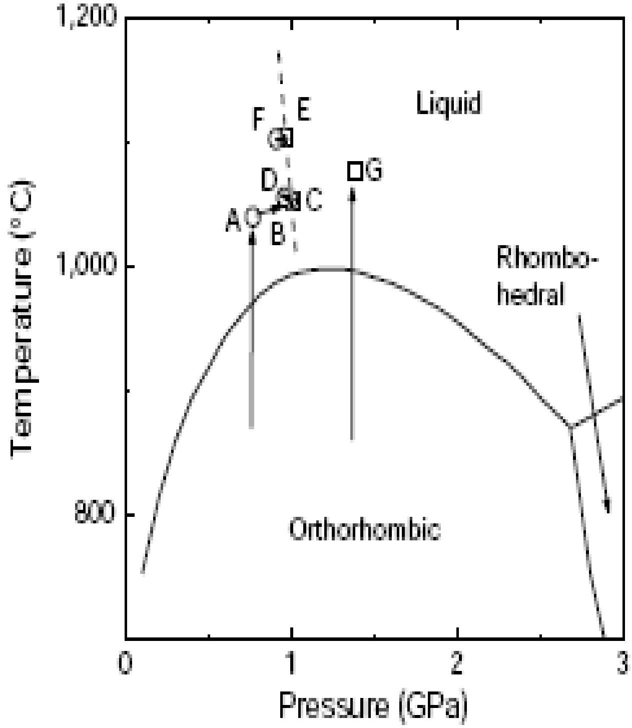

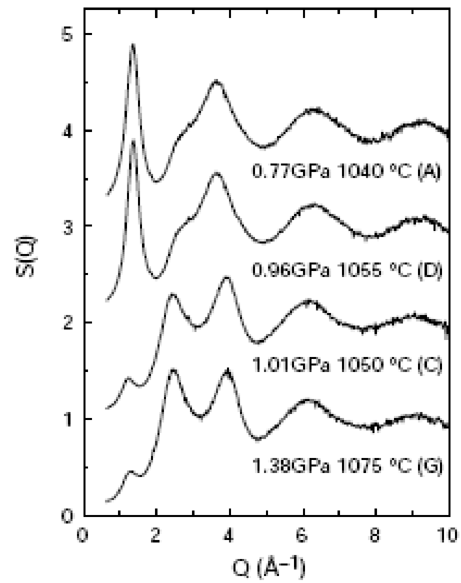

Figure 2 Structure factor, $S(Q)$, for liquid P at several pressures. The letters in parentheses indicate data points in Fig. 1 where the measurements were performed. Energy dispersive X-ray diffraction was performed using white X-rays. To cover a wide wavenumber range, diffraction data were collected at several diffraction angles, from 3.0° to 20.0°. The structure factor $S(Q)$ was obtained using a program developed by Funakoshi[30] based on an empirical method proposed by Tsuji[15].

- Структурные изменения

В элементарных жидкостях

- Te, As, Sb, Bi, I, Br, S, C

Жидкий азот – аналог жидкого фосфора ?

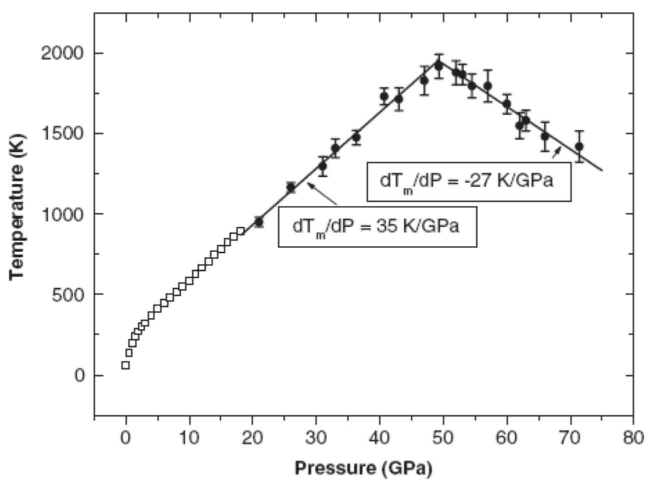

FIG. 2. Melting temperatures of nitrogen at high pressures up to 71 GPa. Dots are data from this work. Open squares are data from Young *et al.* [15]. Solid lines are linear least square fits to our data.

VIEW LETTERS
week ending
30 NOVEMBER 2007

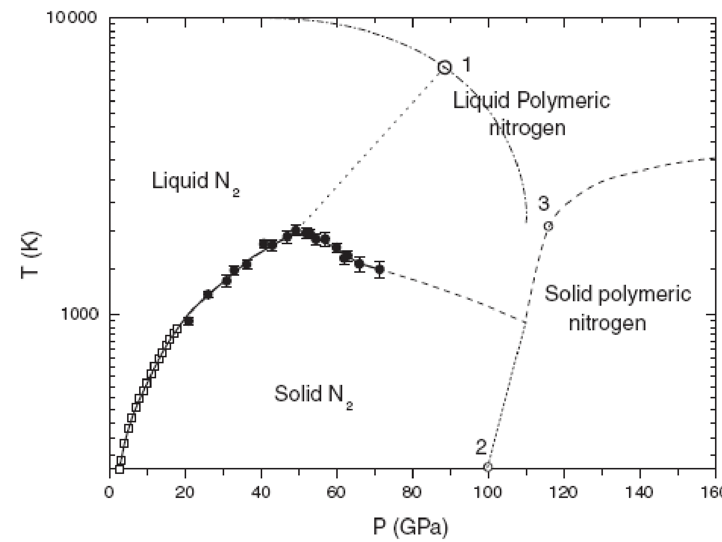

FIG. 3. Proposed nitrogen phase diagram. The solid line traces the experimental melting curve with results from this work (closed circles) and from Young *et al.* [15] (open squares). The reported molecular liquid to polymeric liquid transition is shown by the dot-dash curve [10], which passes through the point labeled 1 at 90 GPa and 7000 K. The modified liquid to liquid transition line is shown by the dotted line, which connects the observed melting-curve maximum to the point 1. The experimental melting curve is extrapolated up to 110 GPa, the transition pressures for the formation of the cg-*N* structure. The solid molecular nitrogen to the solid polymeric nitrogen transition is denoted by the short-dashed line. The point labeled 2 is the equilibrium pressure of the transition between molecular and nonmolecular nitrogen [8]. The dashed line gives the probable melting line for the polymeric nitrogen which passes through 2000 K, which is the melting temperature of nitrogen at 115 GPa, as observed by Eremets *et al.* [9].

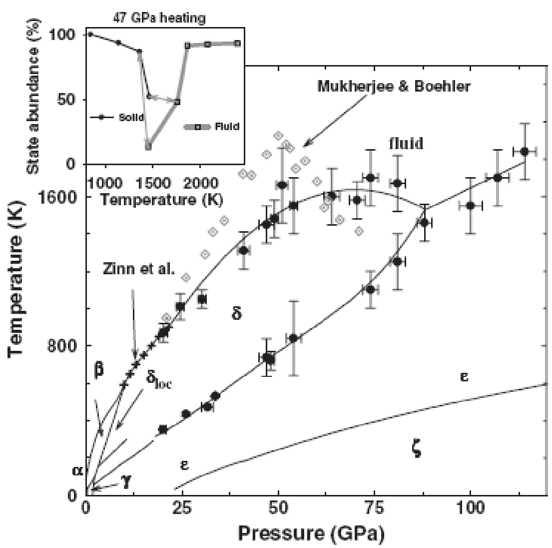

Превращения в расплавах галогенидов: ZnCl2

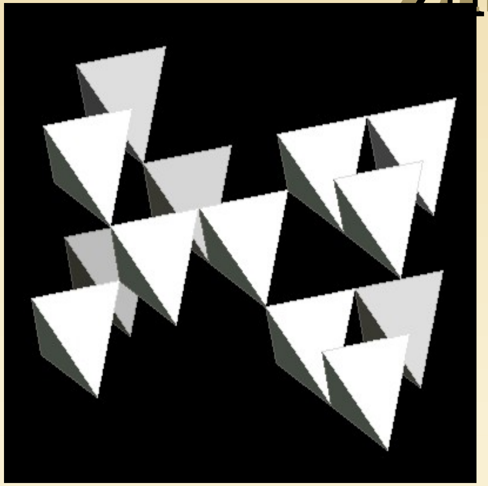

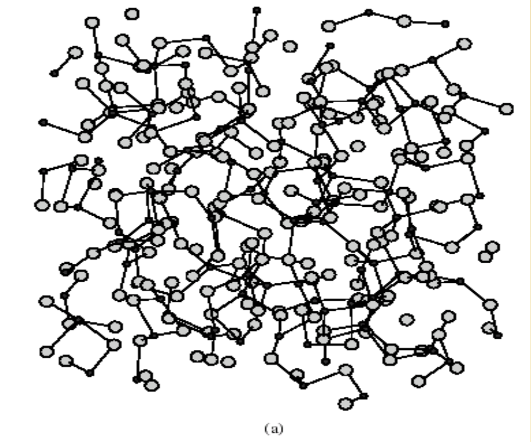

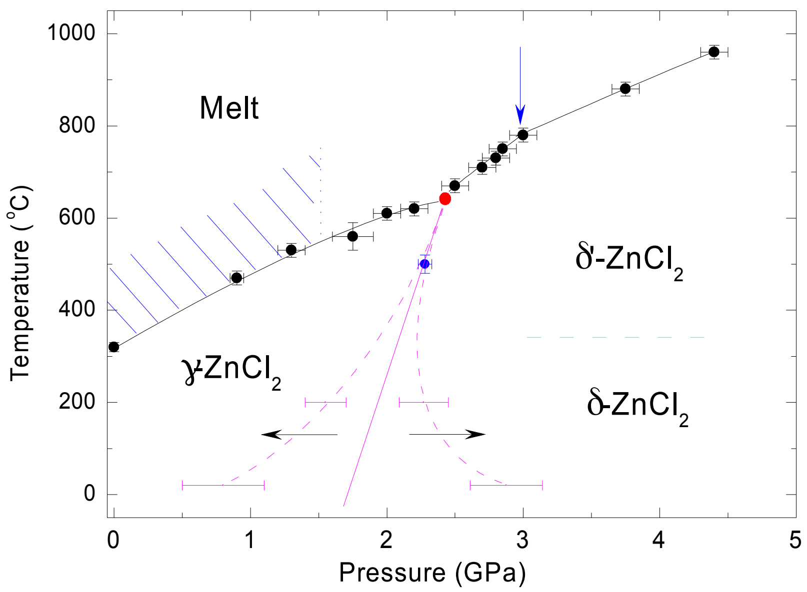

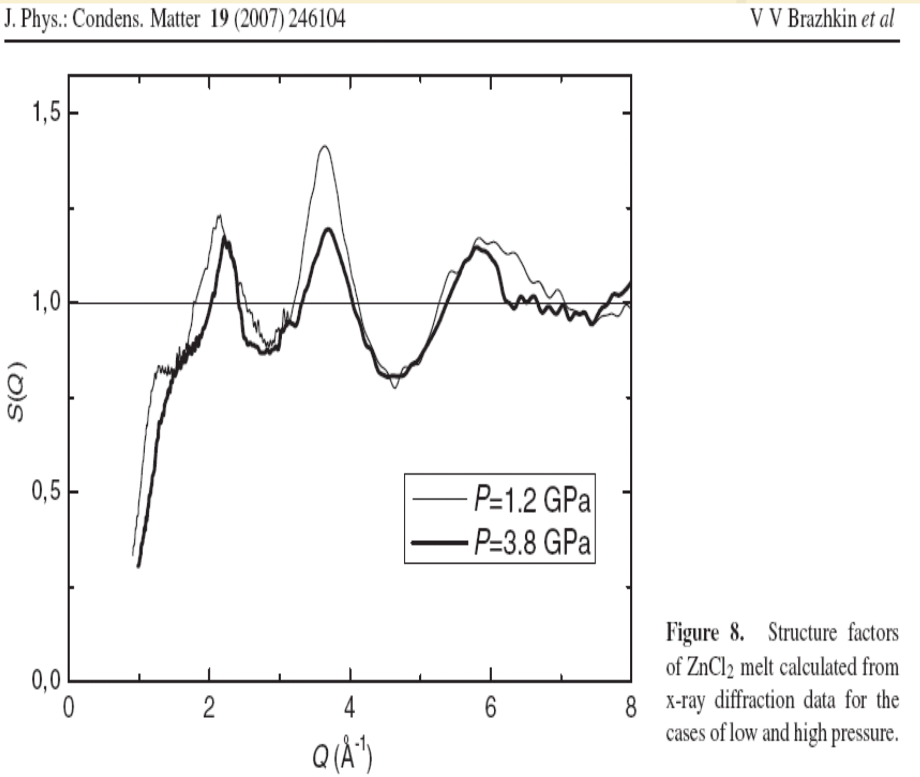

Figure 8. Structure factors of $ZnCl_2$ melt calculated from x-ray diffraction data for the cases of low and high pressure.

Превращения в расплавах галогенидов AlCl3

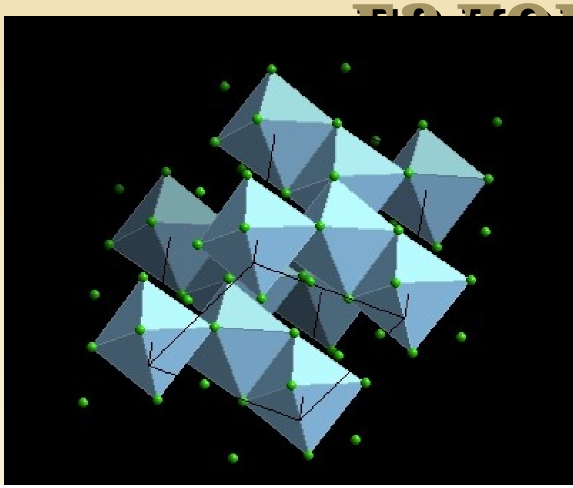

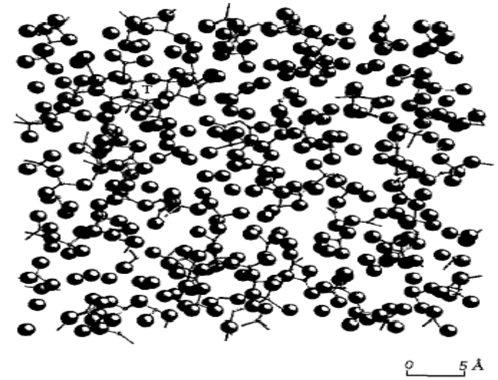

Figure 11. A 'slice' through a model-II RMC configuration corresponding to that for model I in figure 9 (same thickness, plane etc). Although there are now clearly more instances of edge sharing, the overall impression is still of chains of mainly corner-linked, tetrahedral units. What appears to be a 'triplet' of Al atoms (forming part of a larger connected unit) is visible in the top left of the picture and is marked by the symbol 'T' in the middle of the distinctive 'triplet' loop.

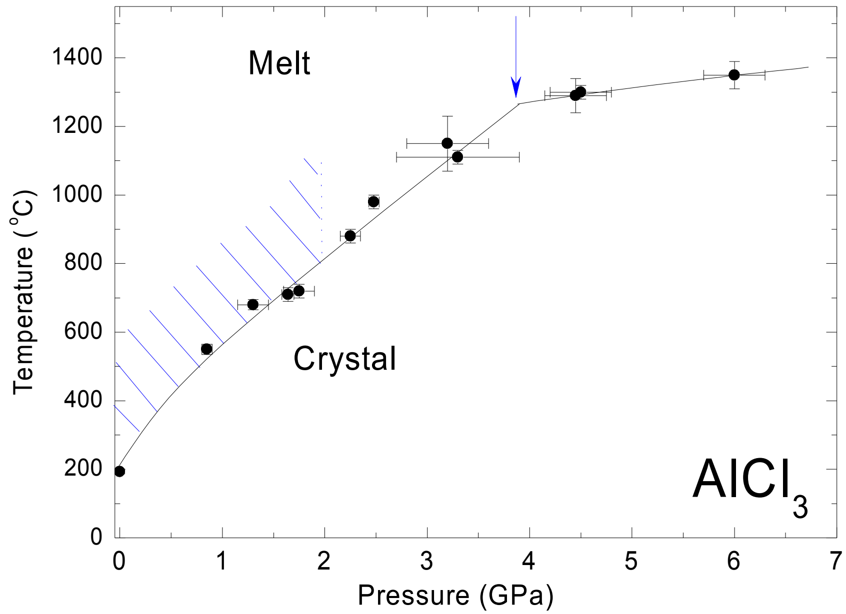

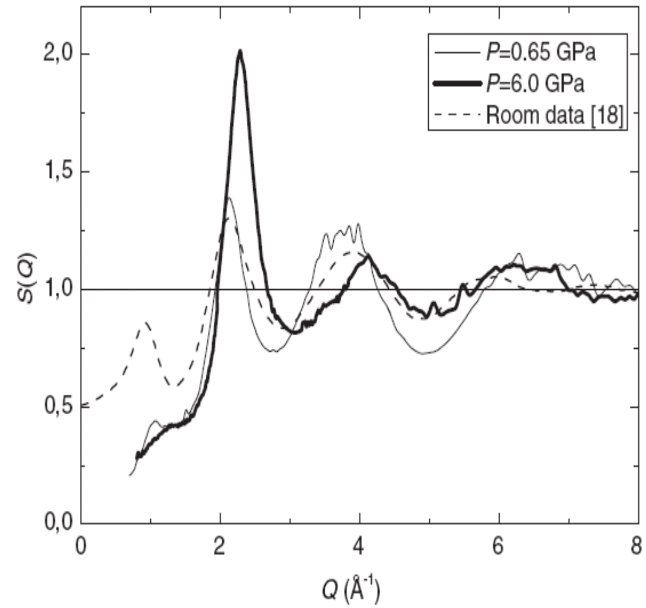

Figure 7. Structure factors of $AlCl_3$ melt calculated from x-ray diffraction data for the cases of low and high pressure. The structure factor at room pressure, measured by the time-of-flight neutron diffraction, is taken from [18].

Превращения в расплавах галогенидов AgI

J. Phys.: Condens. Matter 19 (2007) 076104 H Arima *et al*

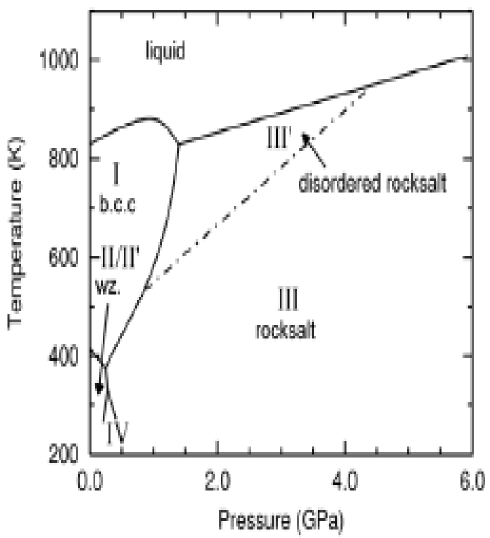

Figure 1. *P–T* phase diagram of AgI after [6–10]. The solid lines are the thermodynamic equilibrium phase boundaries, while the chained line indicates the approximate boundary between AgI-III and AgI-III′ [8–10].

J. Phys.: Condens. Matter 19 (2007) 076104 H Arima *et al*

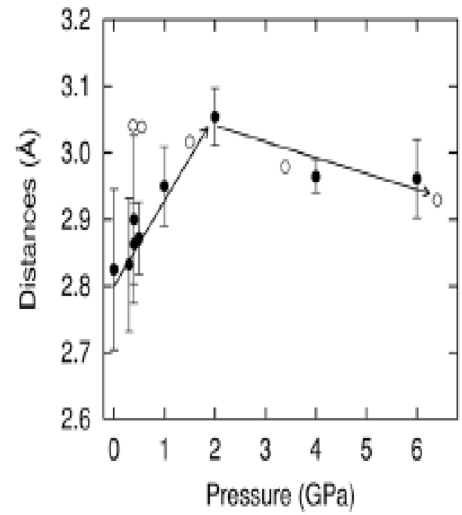

Figure 4. Pressure variation of the first-neighbour I–Ag bond lengths in liquid AgI at 1000 K (solid circles). For comparison, values of the rocksalt-structured phase AgI-III at room temperature [23, 24] (open circles) are also shown. The arrows are only a guide for the eye.

SnI4, SnBr4

AsS (realgar)

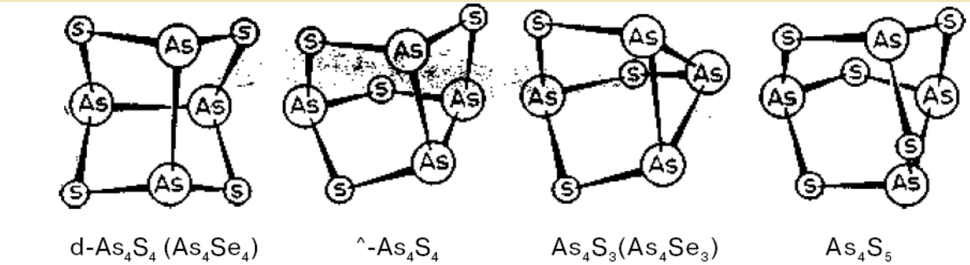

Рис. 3.31. Сульфиды мышьяка с молекулярной структурой [346].

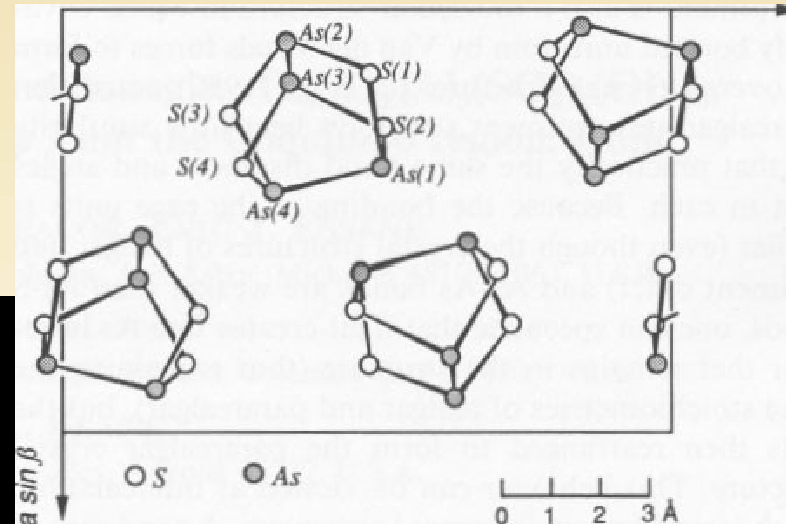

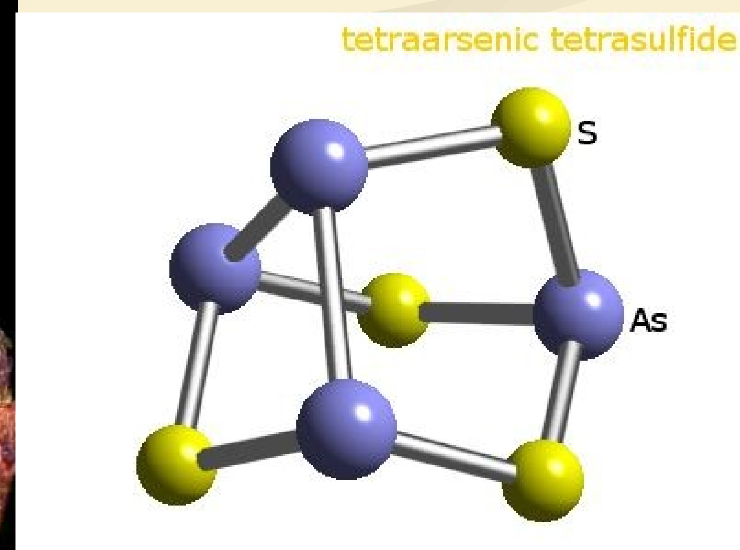

AsS -3 фазы в одном расплаве

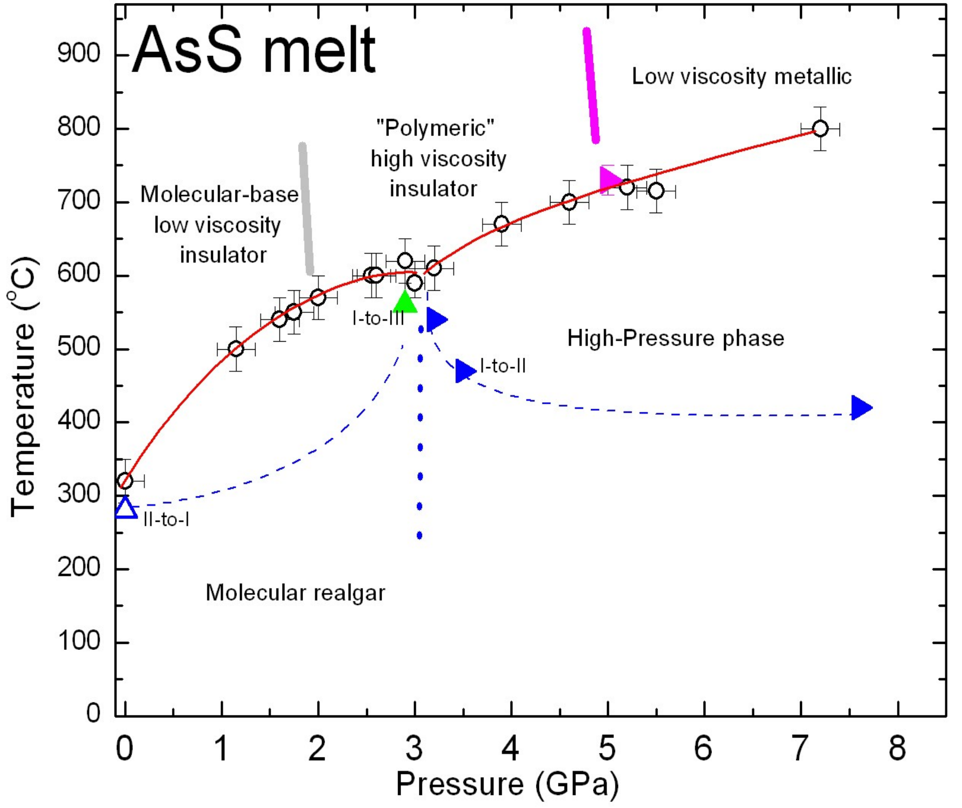

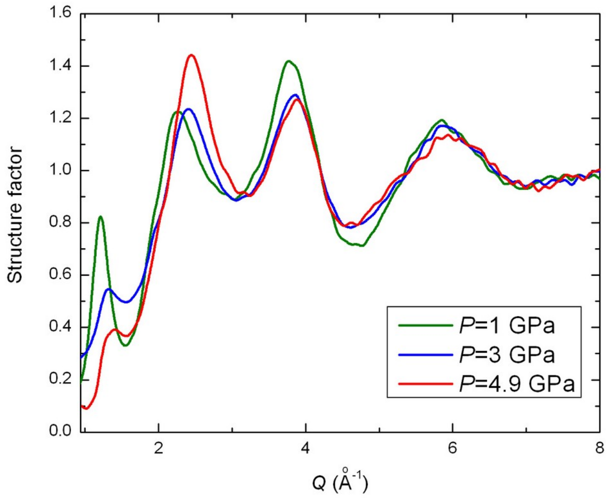

AsS – структура и электросопротивление

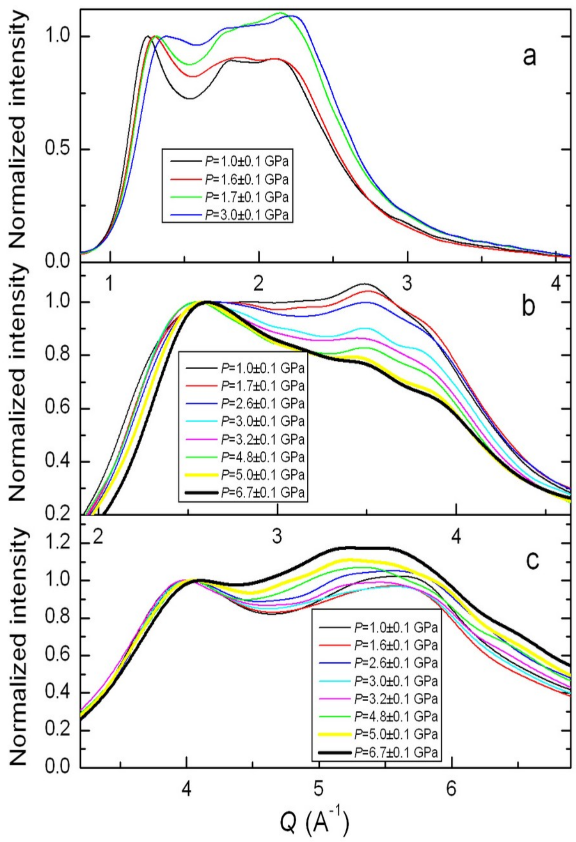

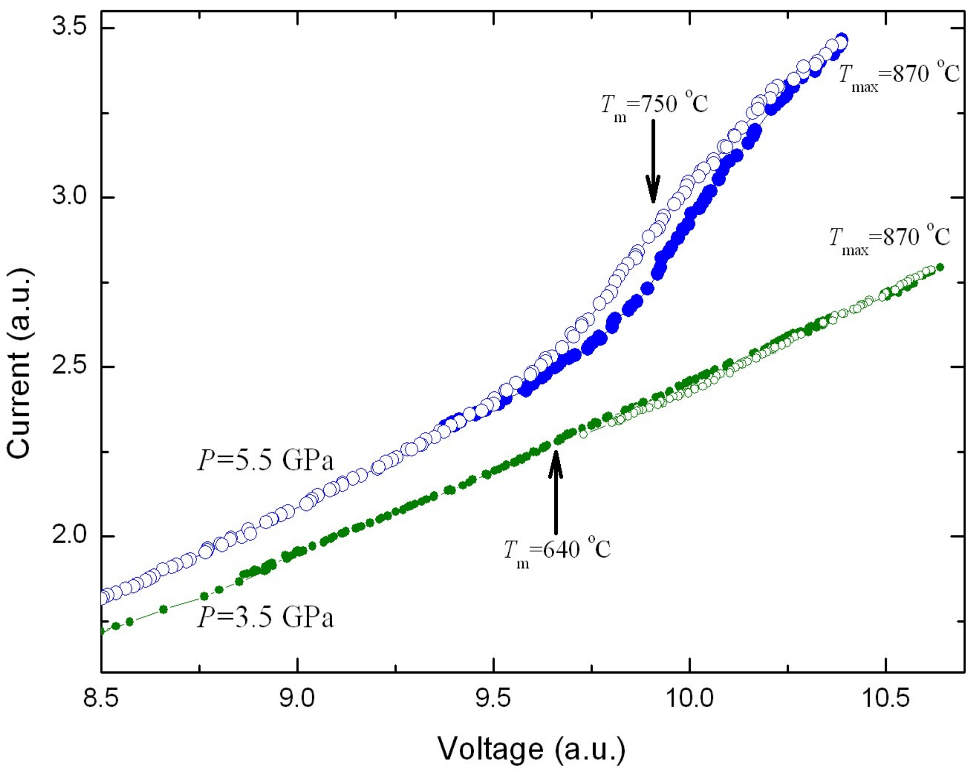

AsS вязкость

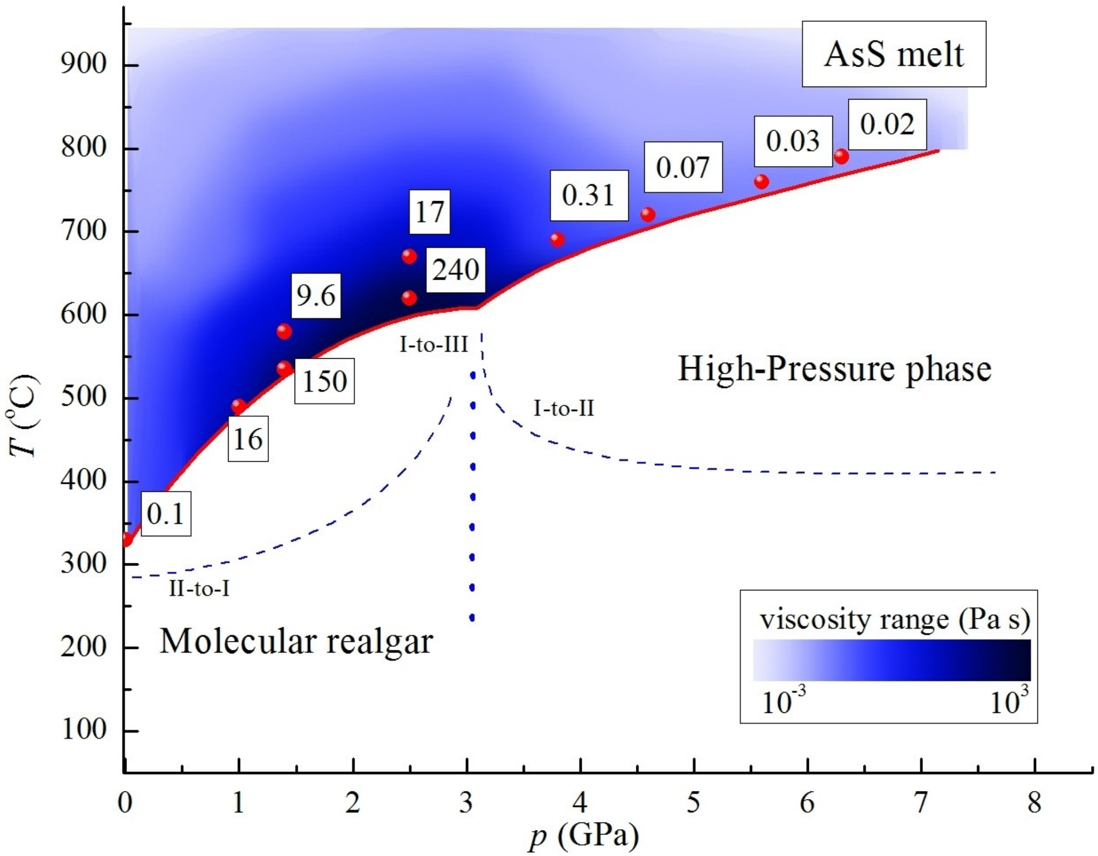

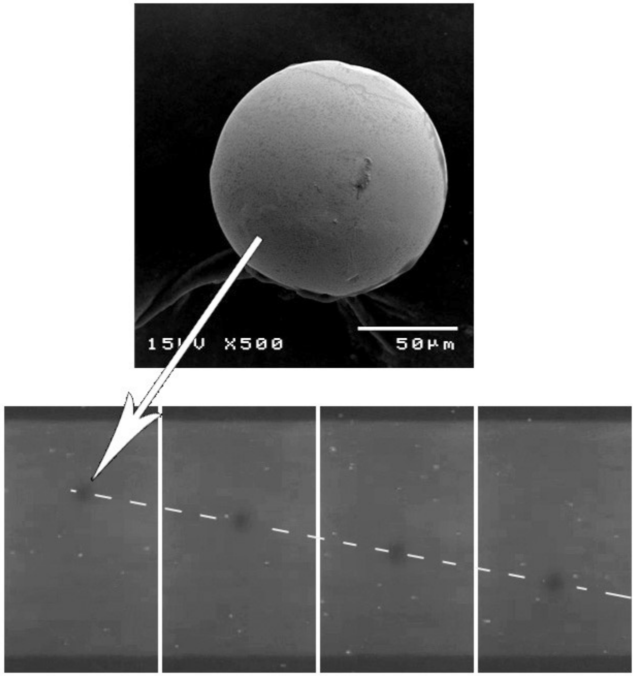

Превращения в расплавах халькогенидов: CdTe

PHYSICAL REVIEW B **73**, 054203 (2006)

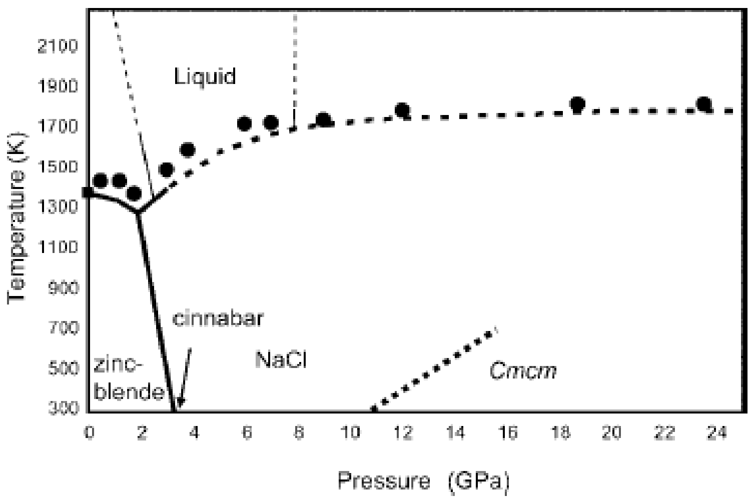

FIG. 1. Previously reported phase diagram of CdTe and the experimental PT conditions in our EDX experiment. The phase boundaries shown by solid bold lines are based on Refs. 28 and 41, and 64. The pressure of the NaCl-orthorhombic *Cmcm* transition is based on Ref. 29 and the slope is speculated from that in ZnTe (Ref. 65). The melting curve above 4 GPa is estimated from the results of the present study. The thin lines show the boundaries between liquid forms estimated from the results of this study.

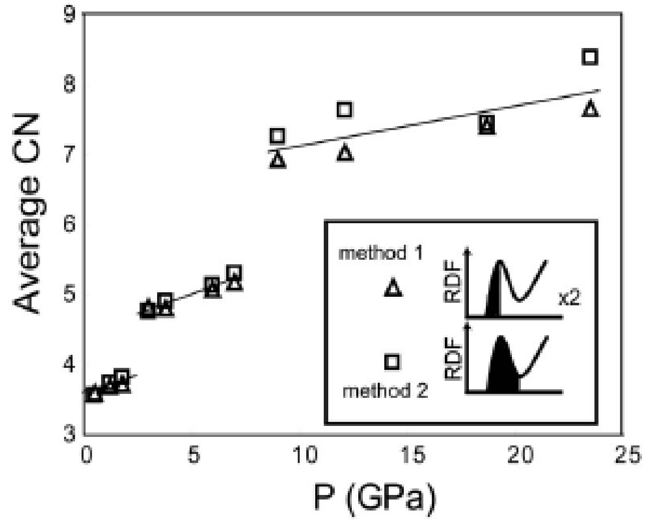

FIG. 4. Average CN for *l*-CdTe at high pressures. Thin lines are only to guide the eyes. The inset shows two methods used in the calculation of CN. In method 1, CN is defined as twice the integrated RDF in the *r* region between the right-hand edge of the first peak r_0 and the *r*-value at the top of the peak. In method 2, CN is defined as the integrated RDF in the region between the r_0 and the *r*-value at the first minimum.

Broad Phase Transformations in SiO2 and GeO2 melts

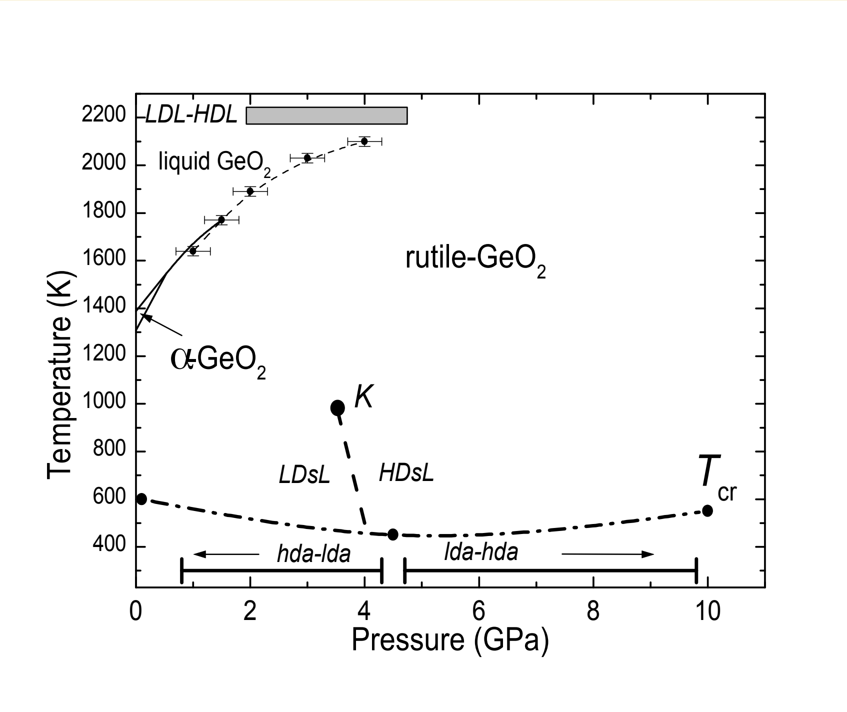

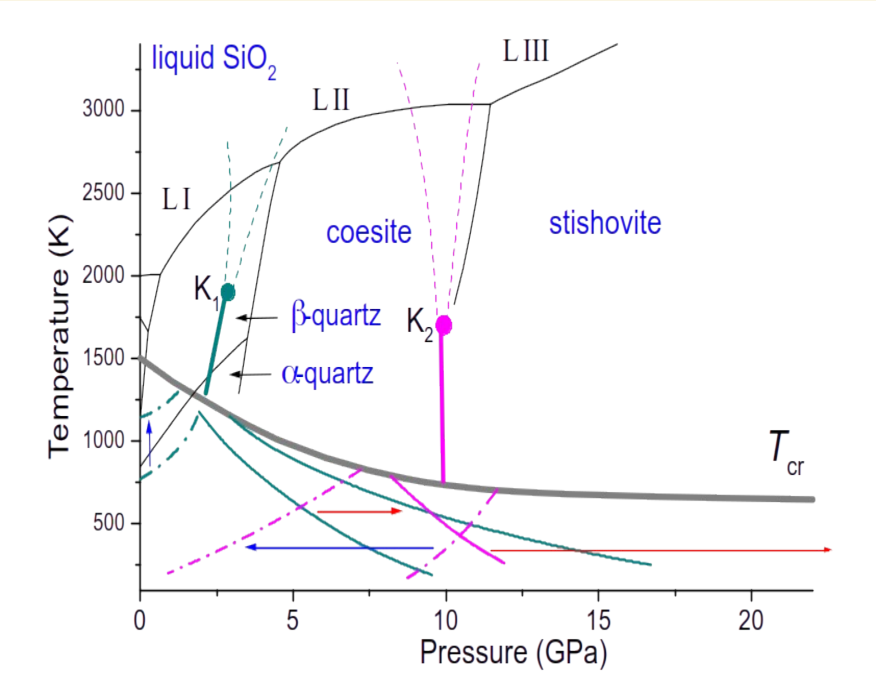

B2O3 crystals, glass and liquid

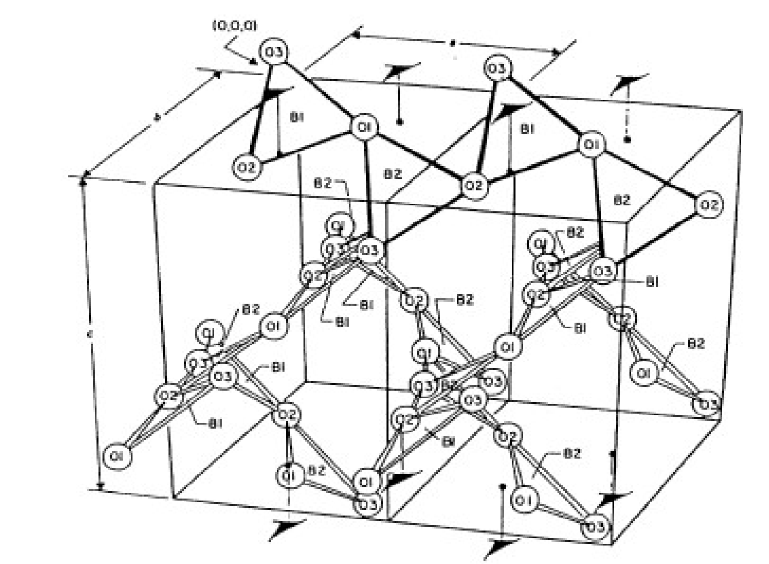

FIG. 1. The B_2O_3-I structure (Ref. 15).

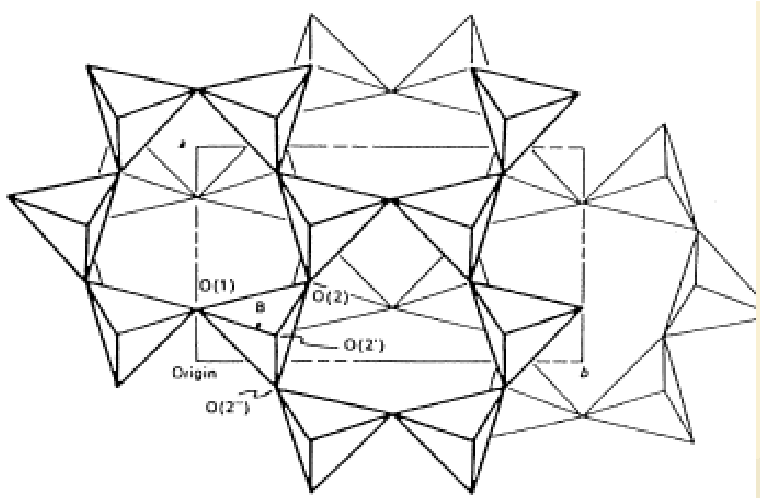

FIG. 2. The B_2O_3-II structure (Ref. 16).

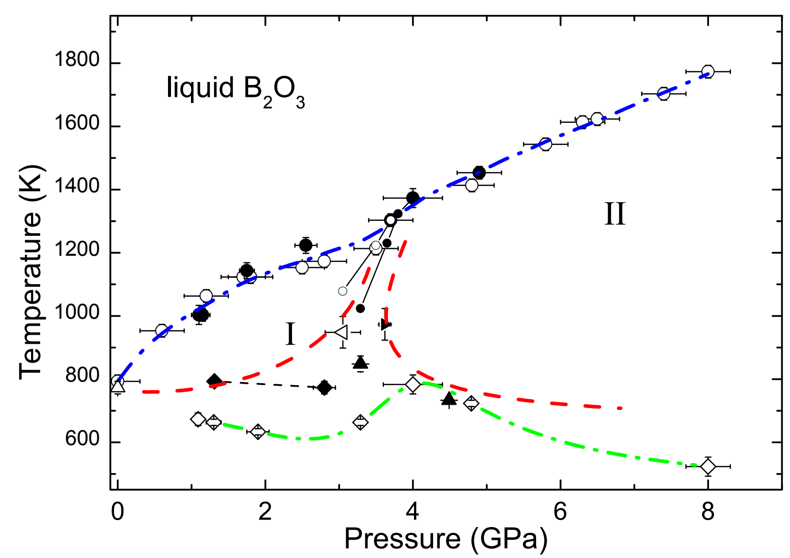

Структура и вязкость в расплаве B2O3

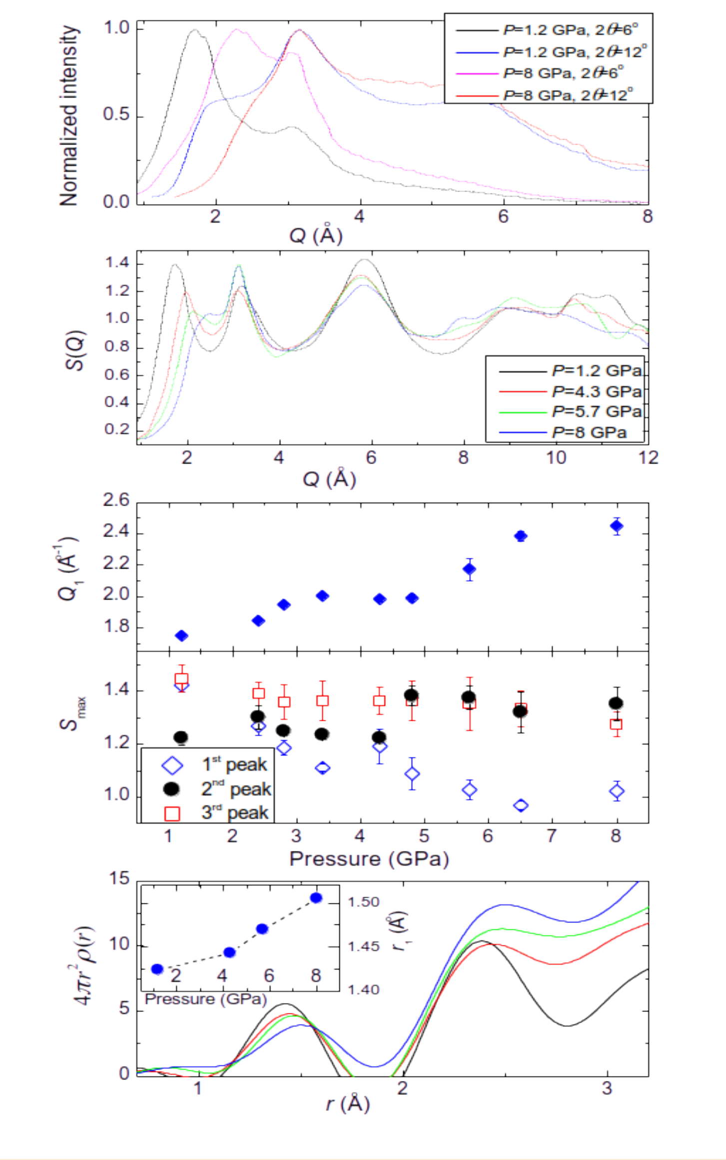

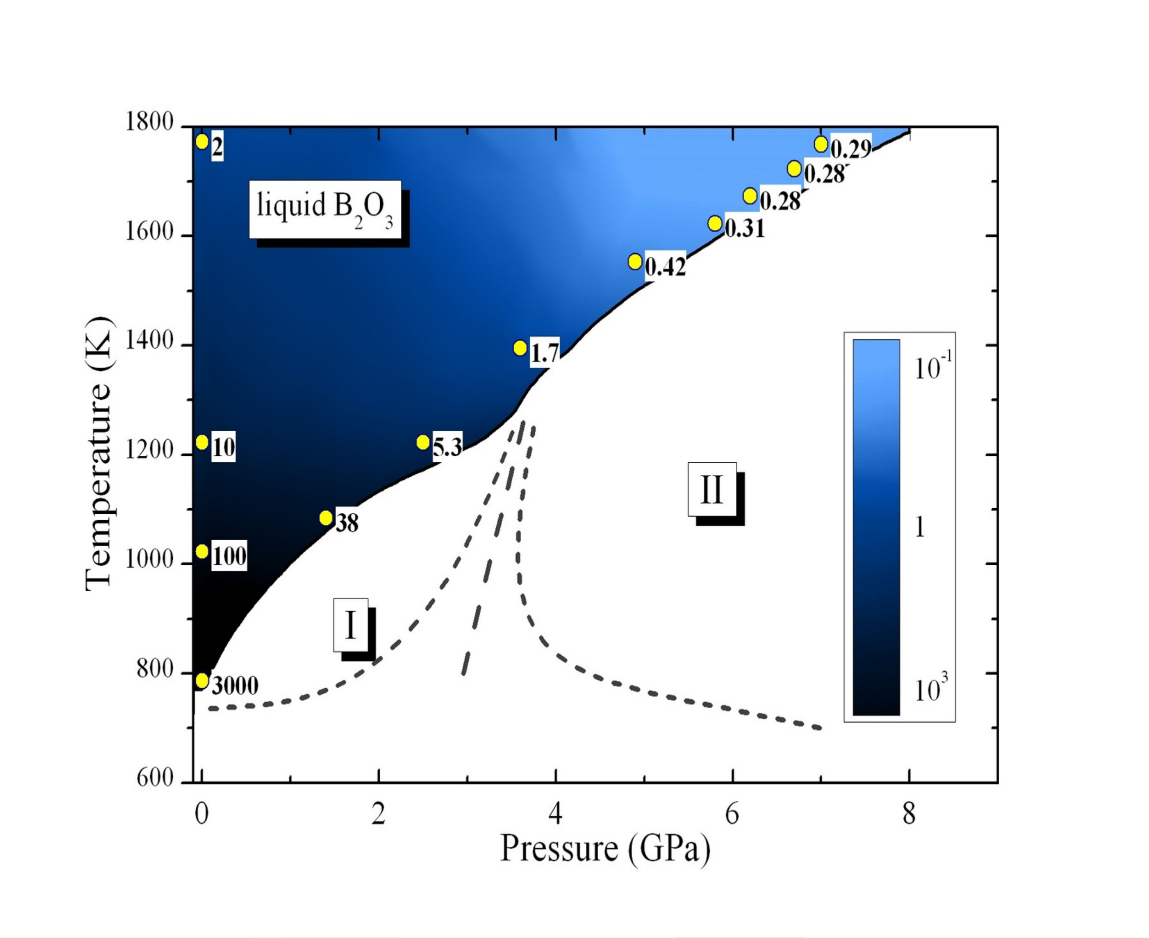

Стекла и аморфные фазы: H_2O

Превращения в оксидных стеклах: SiO2

Измерения поведения плотности стекла при сжатии с помощью тензодатчика

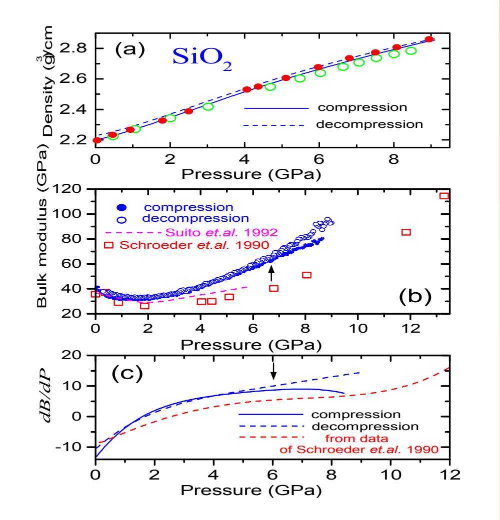

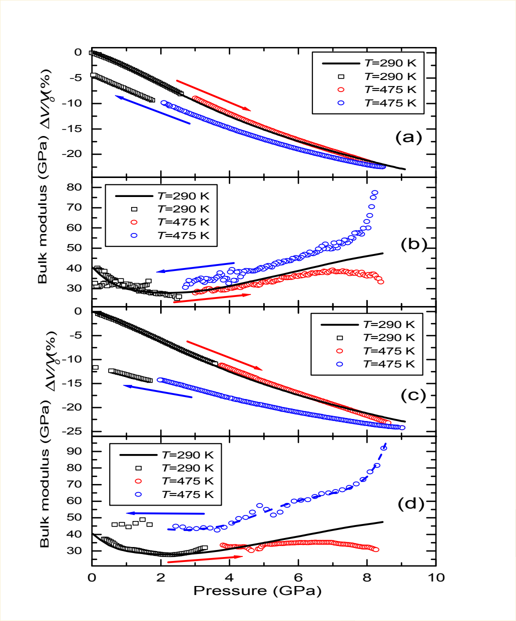

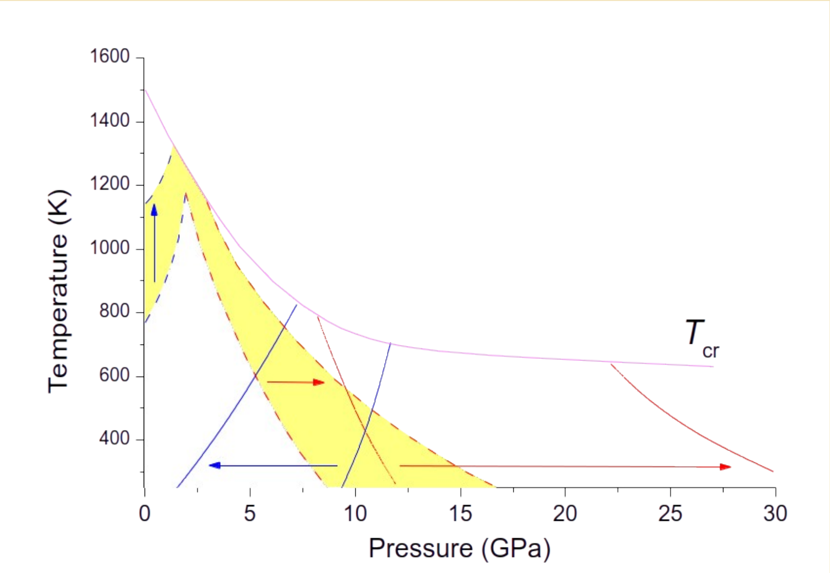

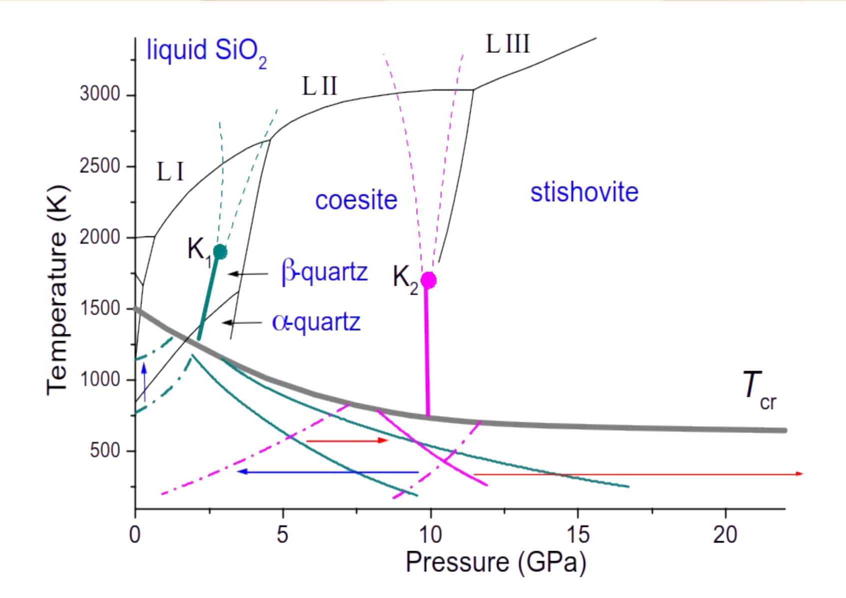

2 размытых превращения в a-SiO2

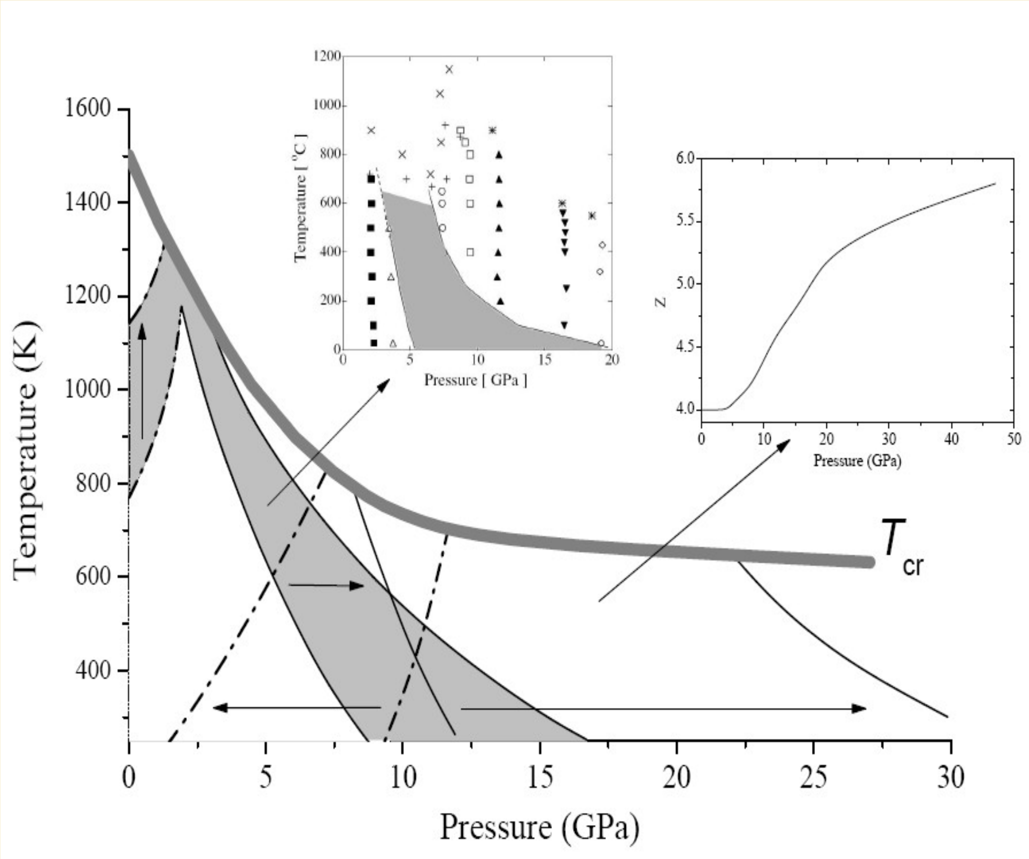

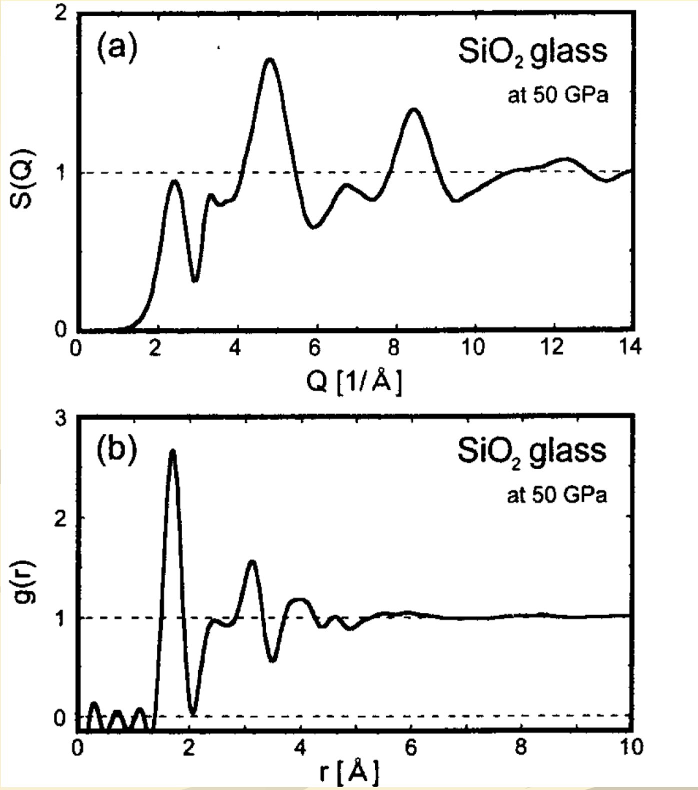

Превращения в оксидных стеклах: GeO2

Измерения поведения плотности стекла при сжатии с помощью тензодатчика

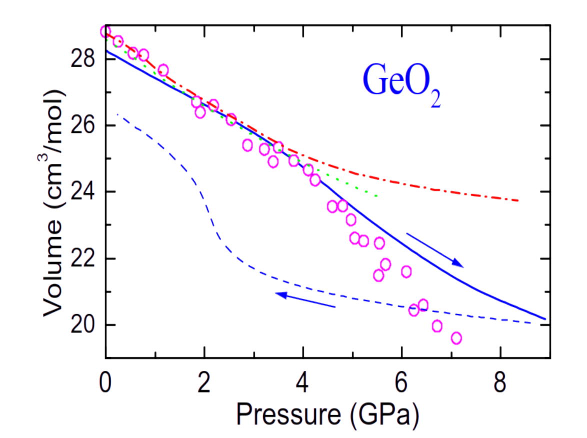

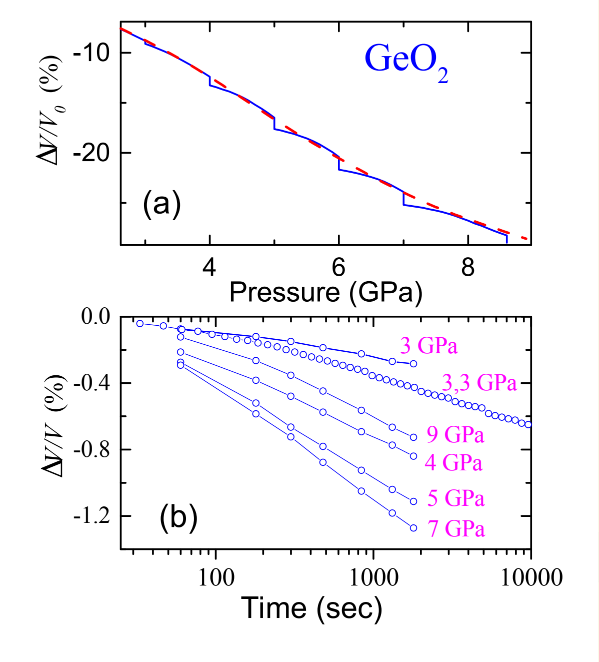

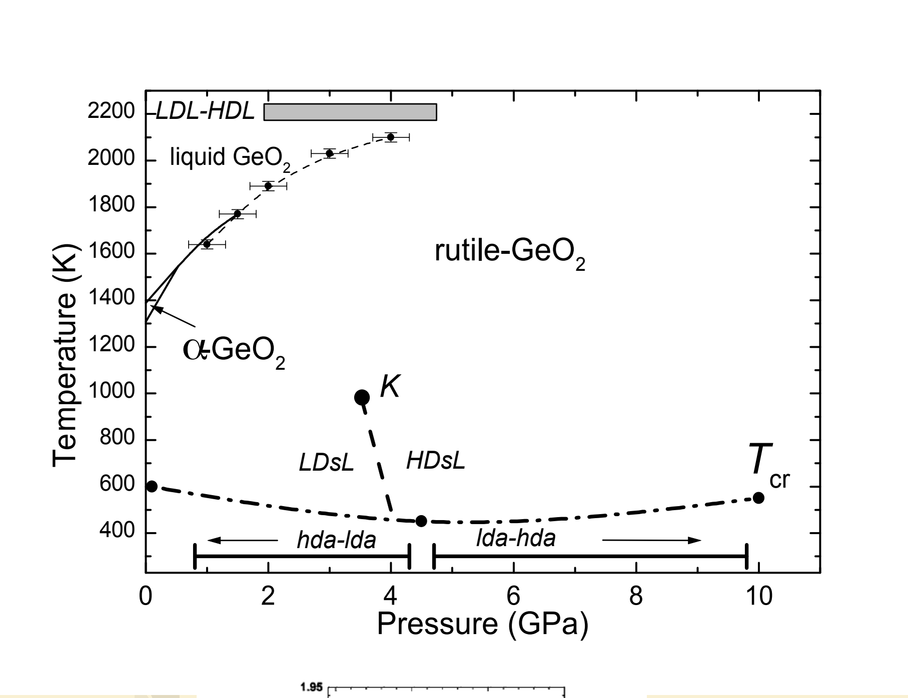

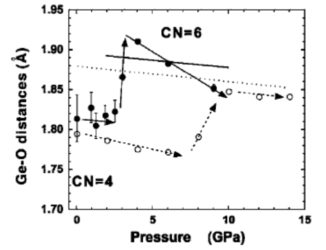

FIG. 4. Variation of the first-neighbor Ge-O distances in the present liquid germanate at 1273 K (solid circles) and Li_2O-4GeO_2 glass at room temperature (open circles). Errors for the distances are estimated from the statistical fitting errors. The relatively large errors in the low pressure region, where $MoSi_2$ heaters were used, are given rise to by the data analysis of the two-phase mixture due to the partial decomposition of GeO_2. The arrows are only guides for the eye. CN indicates the coordination number. Averaged Ge-O distances (four short bonds and two long bonds in distorted GeO_6 octahedron) in the rutile-type crystalline GeO_2 at room temperature and 1273 K are shown by dashed and solid lines, respectively. The compression curves are calculated using room-temperature compression data [15] and a room-pressure thermal expansion coefficient [16].

Превращения в оксидных стеклах: B2O3

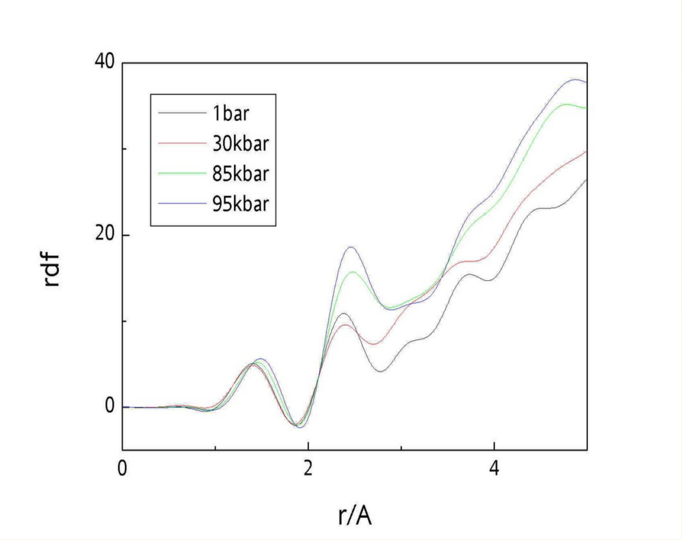

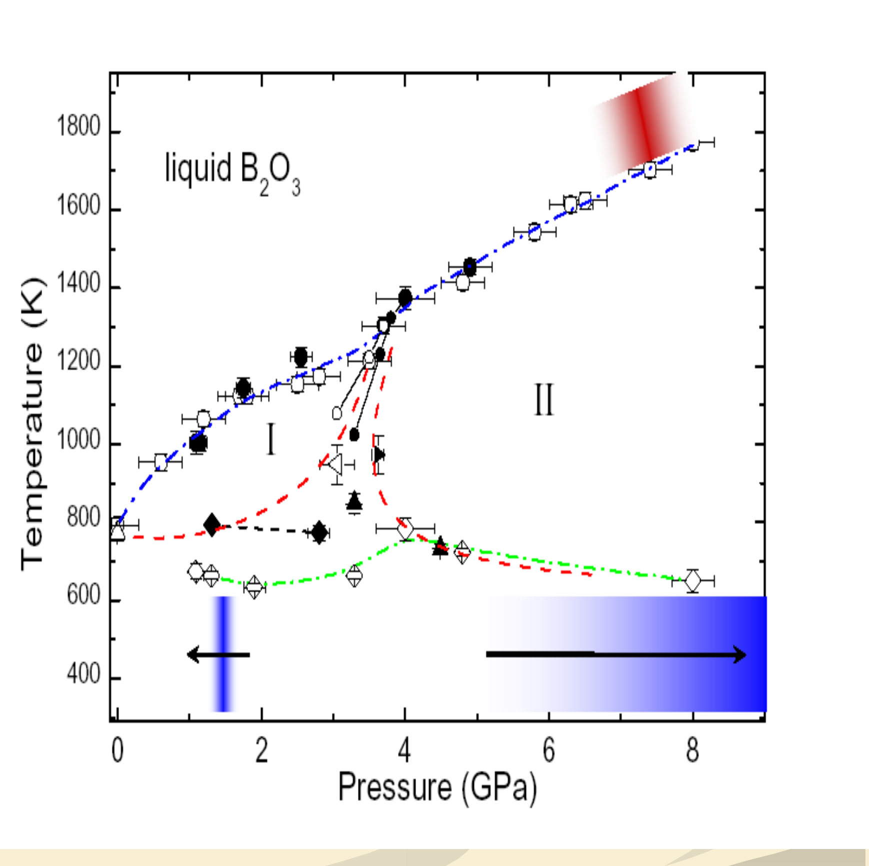

Структурные исследования стекла

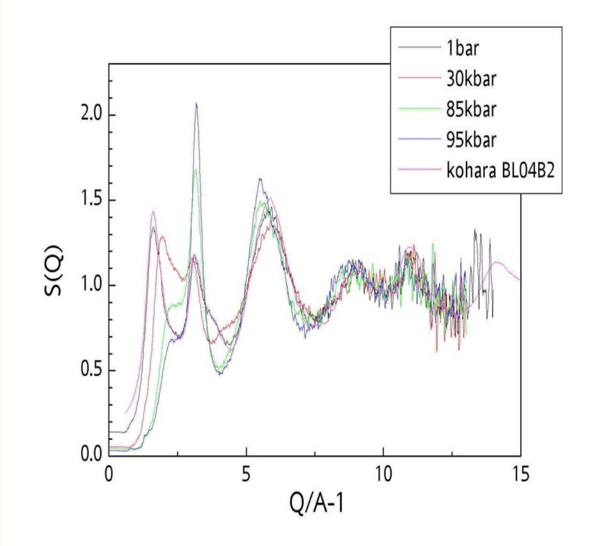

B2O3-структурные исследования и моделирование

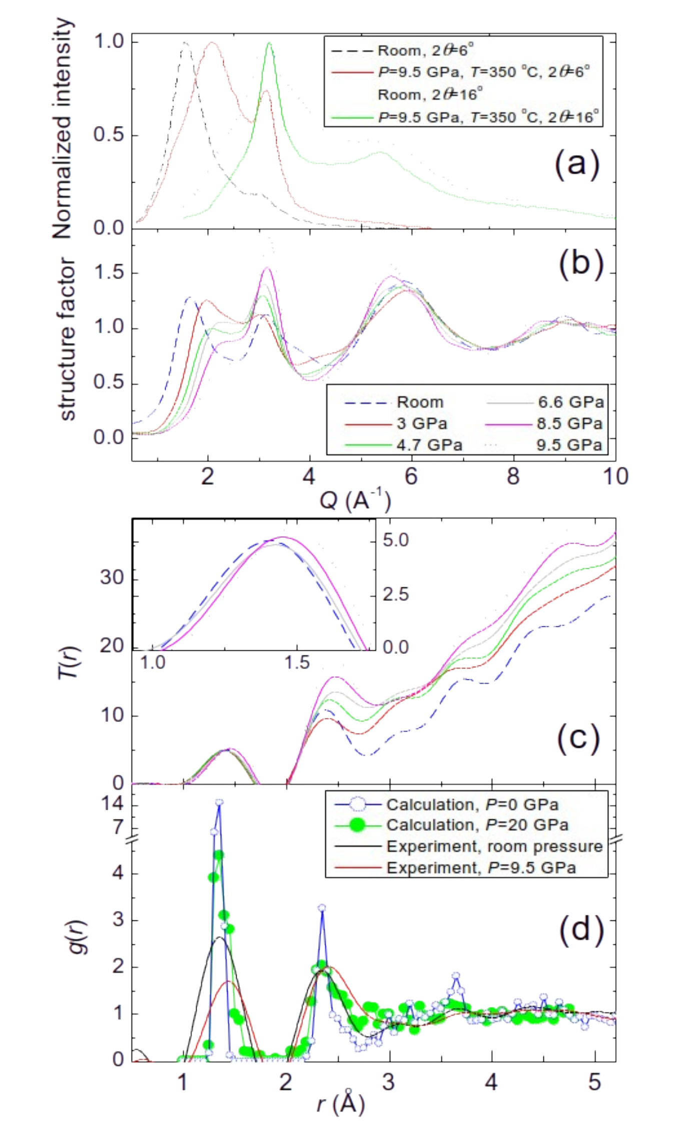

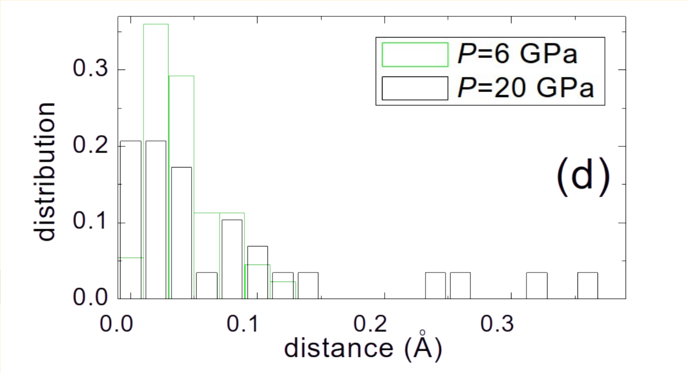

B2O3 – объемные измерения и моделирование

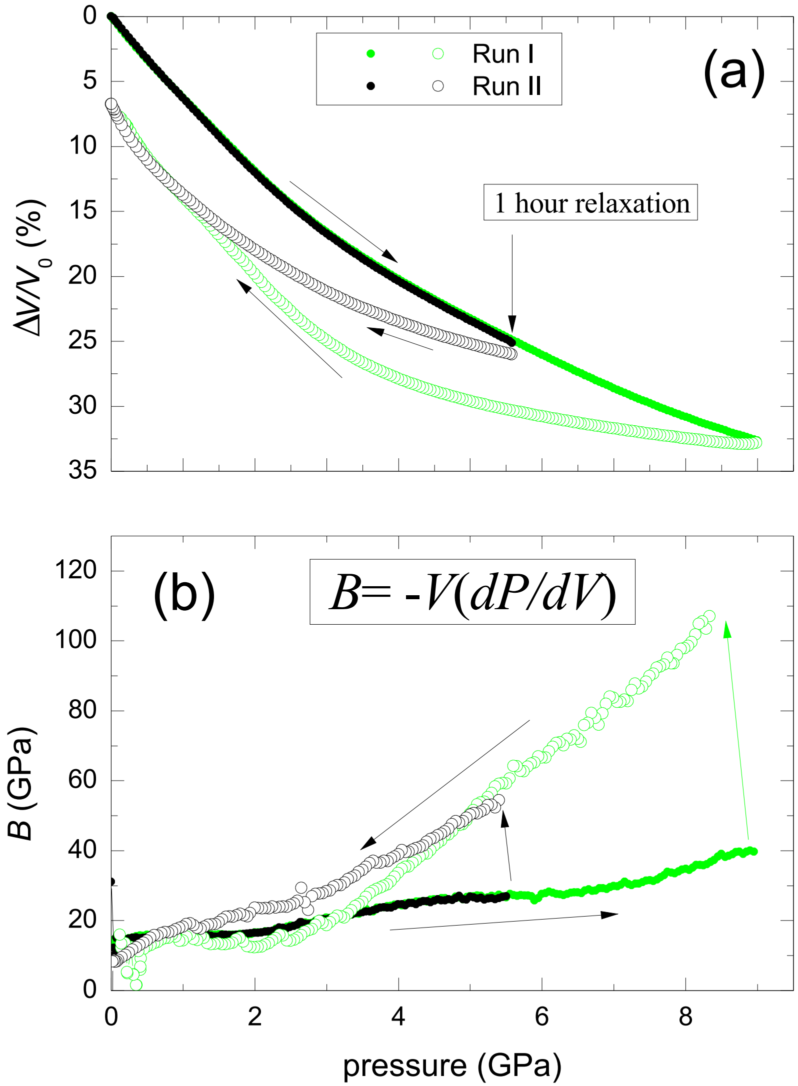

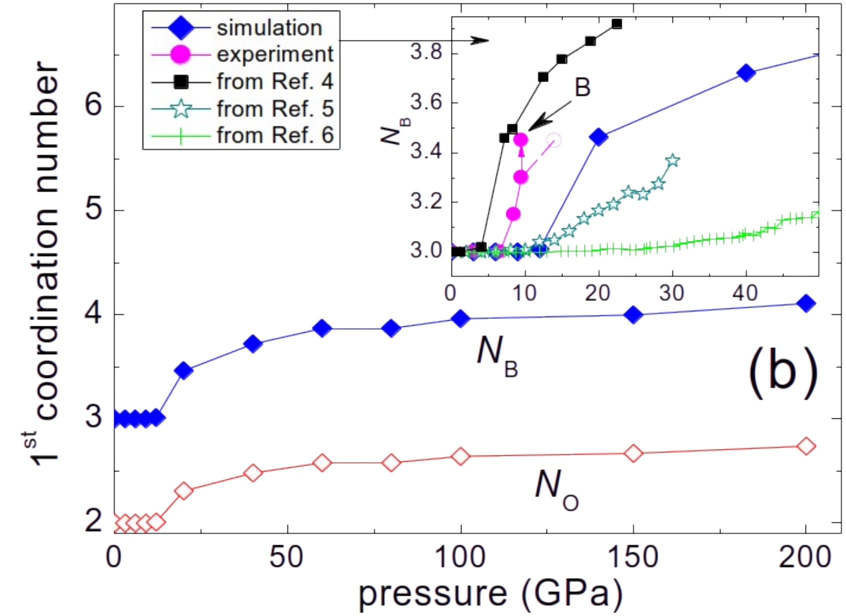

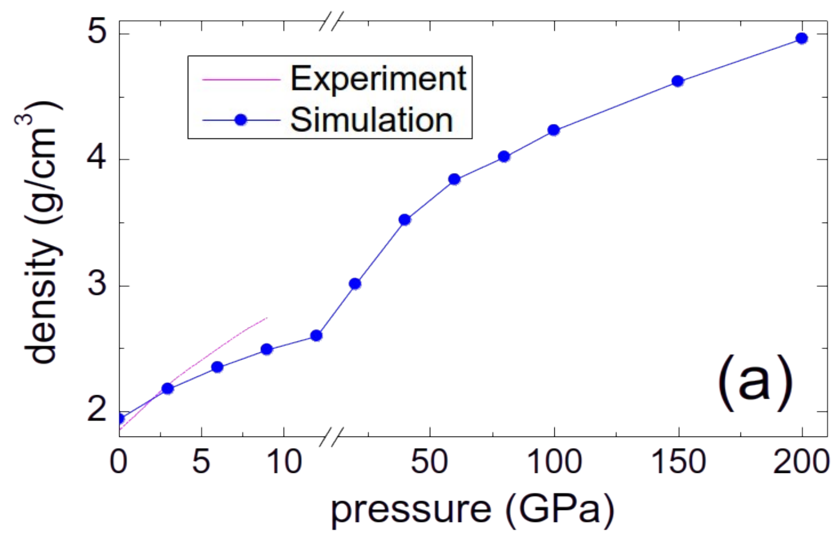

Макроскопическое разделение фаз как свидетельство фазового перехода I-го рода – расплав фосфора

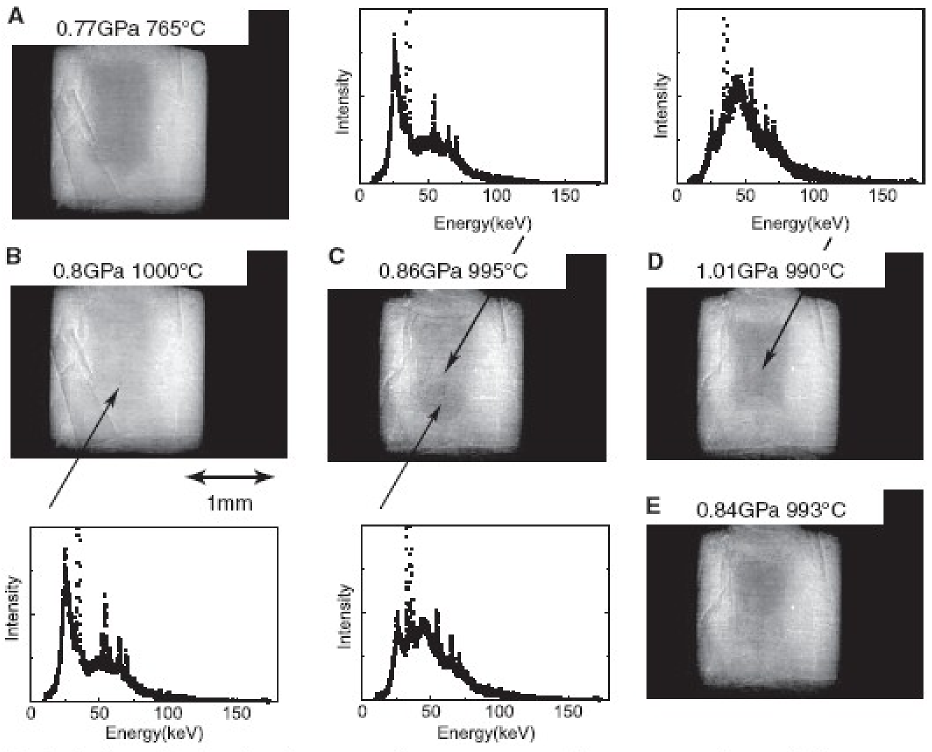

Fig. 1. Radiographs for phosphorus at various pressures and temperatures. Insets indicate x-ray diffraction patterns measured at the positions indicated by the arrows. (A) Black P at 0.77 GPa and 765°C. (B) Low-density fluid phosphorus (LDFP) at 0.8 GPa and 1000°C. (C) A drop of high-density liquid phosphorus (HDLP) in LDFP at 0.86 GPa and 995°C upon compressing. (D) The sample space filled with HDLP at 1.01 GPa and 990°C. (E) A drop of HDLP in LDFP at 0.84 GPa and 993°C upon decompressing. The x-ray aperture was restricted by the anvils. Sharp lines in the radiographs are probably due to textures in the sample assembly.

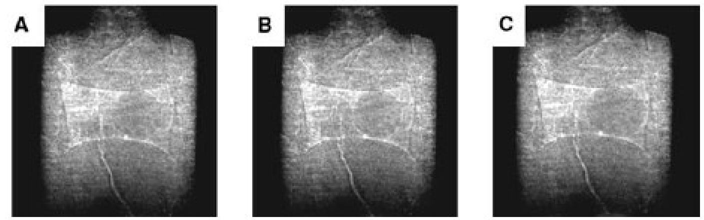

Fig. 2. Snapshots of drops of HDLP in LDFP during the transition. A sample container made of pyrophillite was used. (A) There are a large drop and several small drops. (B) One of the small drops grew into a large drop, and the two large drops are side by side. (C) The two drops coalesced to form a larger drop.

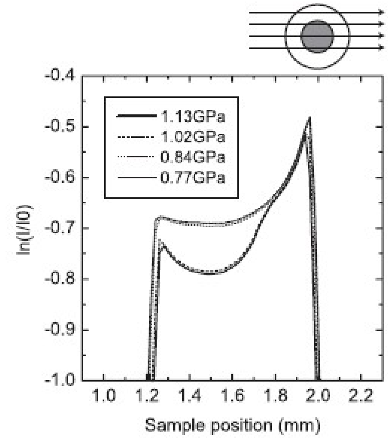

Fig. 3. X-ray absorption profile of liquid phosphorus in a sapphire ring at various pressures and 1000°C. The scan was along an axis parallel to the ring as shown in the upper figure.

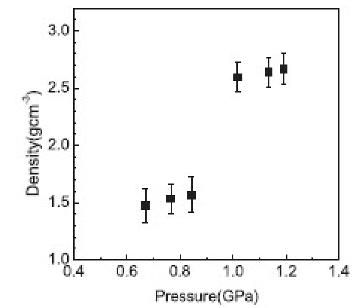

Fig. 4. Pressure dependence of density of liquid phosphorus at 1000°C.

A drop of HDLP sometimes rapidly moved in LDFP and would move from one end of the capsule to the other within a few video frames. LDFP has a low enough viscosity to allow rapid motions, which is consistent with the molecular liquid model. The rapid coa-

VOLUME 92, NUMBER 2 PHYSICAL REVIEW LETTERS week ending 16 JANUARY 2004

Liquid-Liquid Transition in the Molecular Liquid Triphenyl Phosphite

Hajime Tanaka, Rei Kurita, and Hiroshi Mataki
Institute of Industrial Science, University of Tokyo, Meguro-ku, Tokyo 153-8505, Japan
(Received 8 April 2003; published 15 January 2004)

We found both nucleation-growth-type and spinodal-decomposition-type transformation from one liquid state to another in a "molecular liquid," triphenyl phosphite (TPP). Binodal and spinodal temperatures of this transition at ambient pressure were determined by the characteristics of morphological evolution, domain-growth kinetics, and rheological evolution. Furthermore, a distinct thermal signature of the glass transition of a second liquid was also detected in addition to that of an ordinary liquid. These findings strongly suggest the existence of a liquid-liquid transition; more precisely, a transformation of one supercooled liquid to a glassy state of another liquid, in TPP.

VOLUME 92, NUMBER 2 PHYSICAL REV

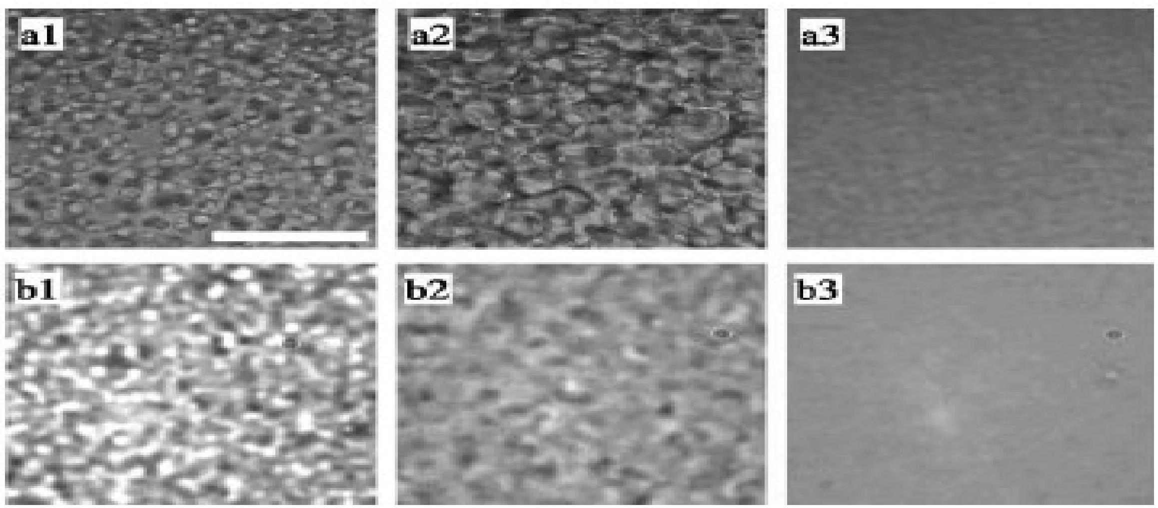

FIG. 1. Pattern evolution observed during the annealing of a supercooled liquid at T_a. (a1)–(a3) are observed with normal microscopy at $T_a = 220$ K at the annealing time $t_a = 60$, 120, and 240 min, respectively. (b1)–(b3) are observed with phase-contrast microscopy for $T_a = 213$ K at $t_a = 120$, 240, and 360 min, respectively. The white bar in (a1) corresponds to 100 μm for (a1)–(a3), while to 20 μm for (b1)–(b3). The sample thickness was 100 μm for (a), while 20 μm for (b).

Два сценария фазовых превращений в неупорядоченных конденсированных средах

- **Резкий или размытый сценарий фазовых превращений в неупорядоченных конденсированных средах определяется соотношением между размером области промежуточного порядка и минимально возможным размером области новой фазы (зародыша).**

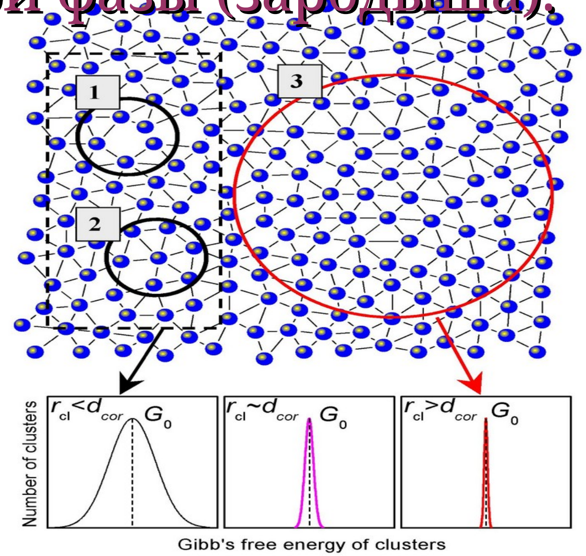

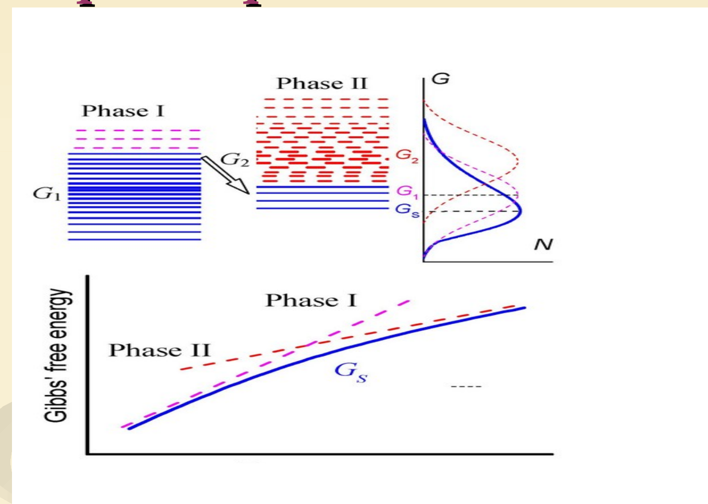

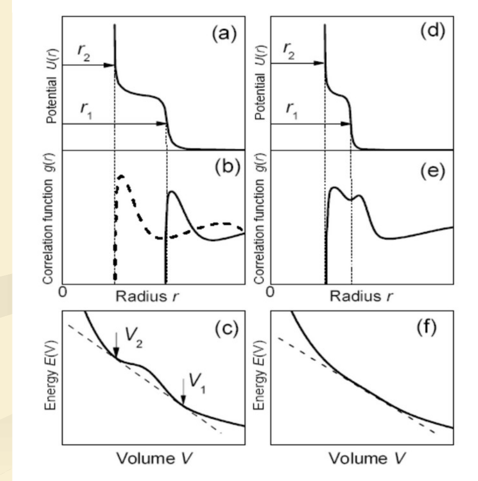

- **Термодинамические причины размытого сценария в рамках кластерной модели**

Выводы

- Исследования структуры и свойств расплавов и стекол под давлением показывают возможность существования как резких, так и размытых фазовых превращений в неупорядоченных средах, сопровождаемых изменениями всех физических характеристик.
- «Редкость» переходов 1го рода??
- Резкие и размытые превращения в неупорядоченных средах находят описание и объяснение в рамках простых моделей. Вместе с тем адекватное теоретическое описание превращений, включая введения адекватного параметра порядка остается под вопросом

Пример использования переходов в расплаве:

AsS стекло

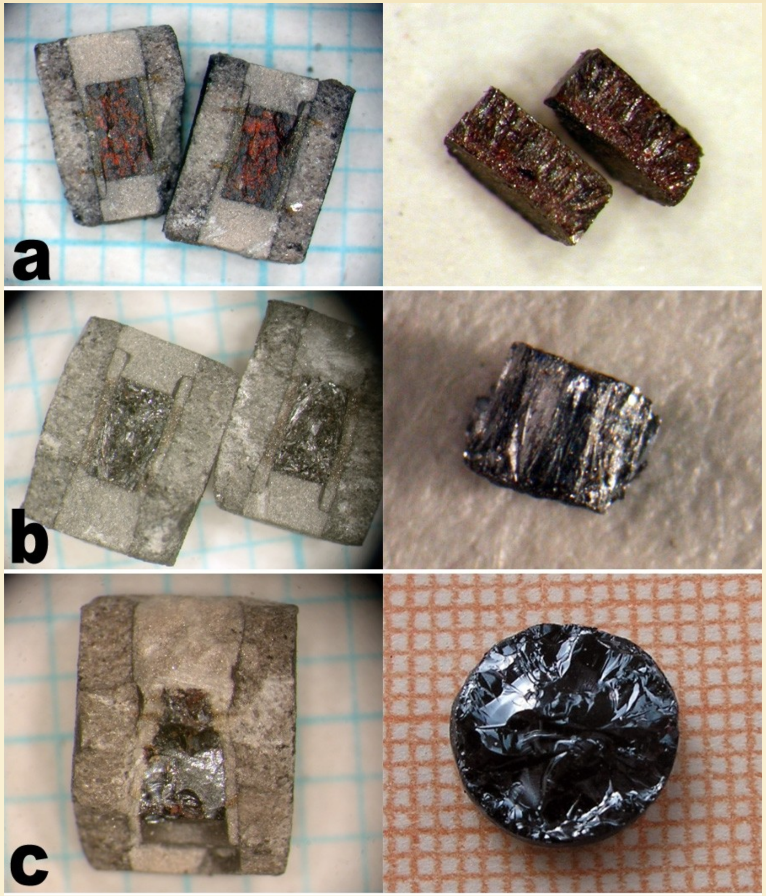

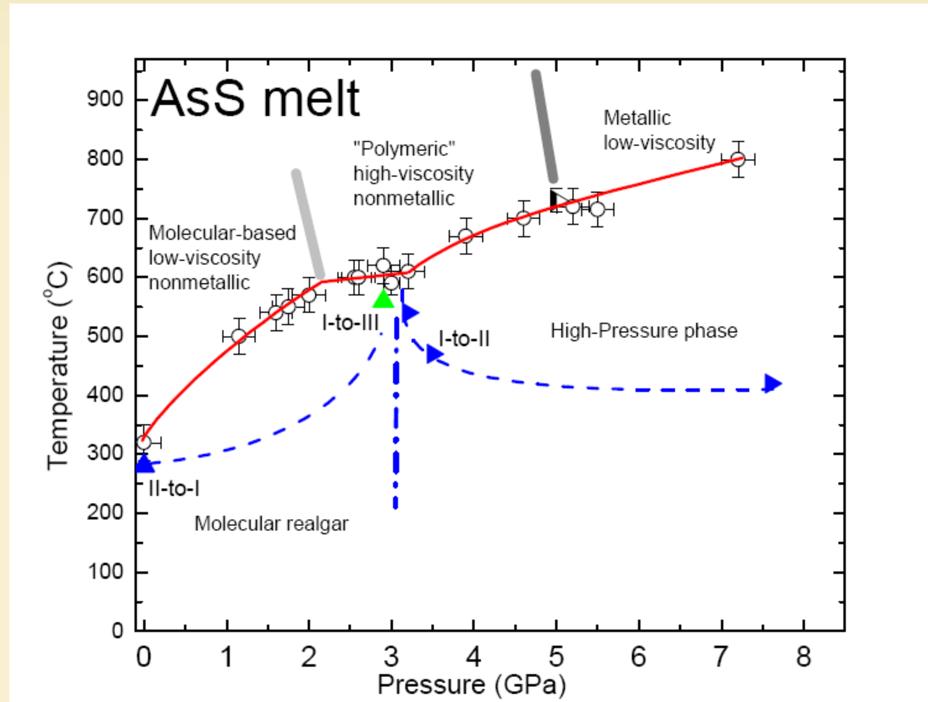

Structure and optical absorption spectra of new AsS glass

Appl. Phys. Lett. **91**, 031912 (2007)

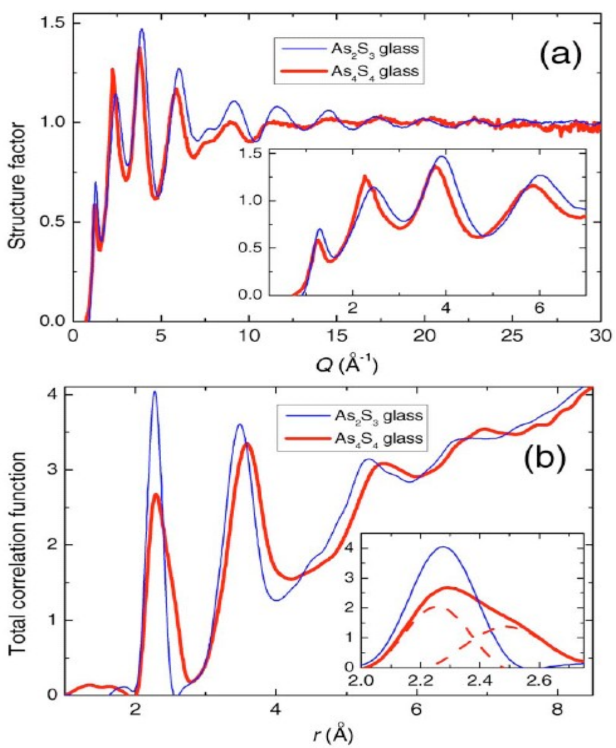

FIG. 2. (Color online) (a) Structure factor and (b) total correlation function obtained by x-ray diffraction for As_4S_4 glass (thick lines) and compared with the data for the canonical As_2S_3 glass from Ref. 21 (thin lines). The insets show the initial parts of the corresponding curves. For the total correlation function, the inset also illustrates two different contributions (dashed lines) to the first coordination sphere of the As_4S_4 glass. The sample of the glassy As_4S_4 was synthesized by quenching from the melt at $P = 3.4$ GPa and $T = 700$ °C.

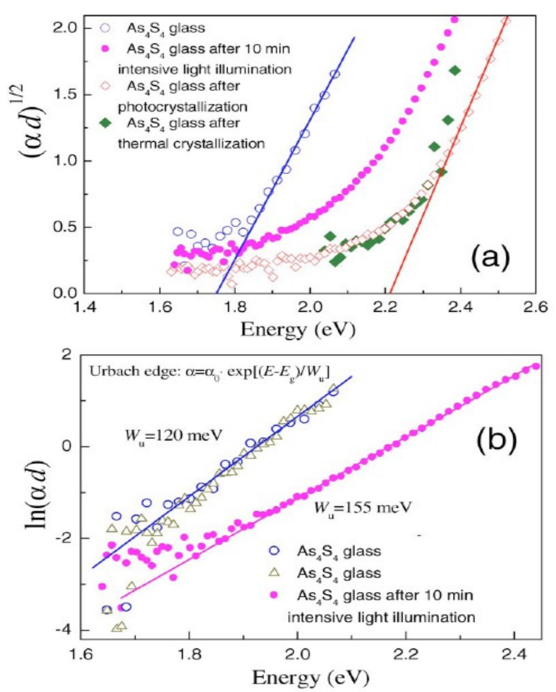

FIG. 3. (Color online) Plots of the optical inverse transmission spectra, for the initial As_4S_4 glass and for the partially crystallized (by 10 min light illumination) sample in different coordinates for determination of the optical pseudogap and the Urbach absorption tail energy. (a) $(\alpha d)^{1/2}$ vs E plot shows the inverse transmission data for the crystalline As_4S_4, obtained by thermal crystallization at 200 °C and by photocrystallization. For the latter, the time of illumination exceeds the time during which we observe the saturation of the photostructural changes in the inverse transmission spectra of the initial glass (~1 h). (b) $\ln(\alpha d)$ vs E plot shows the spectra for two independent As_4S_4 glass samples prepared at the same pressure-temperature conditions (close to those in Fig. 2). The thickness of the samples d was estimated to be 11 μm.

Структурные исследования

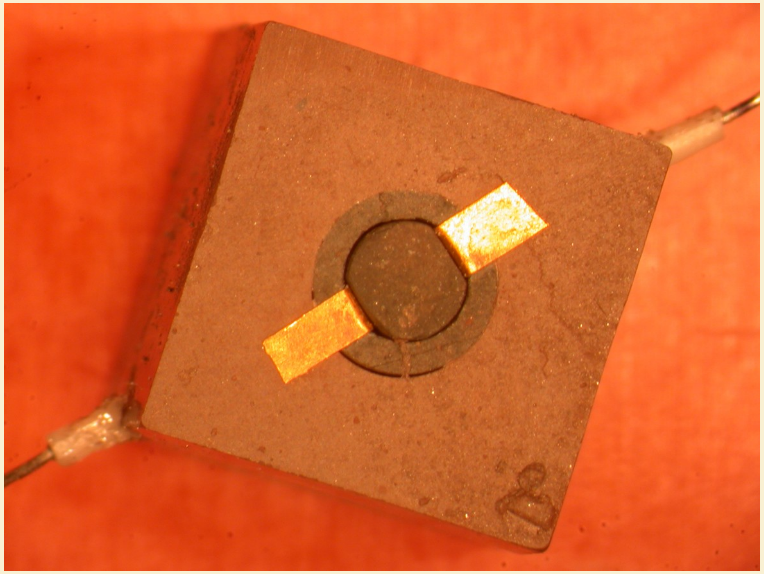

Высокотемпературная сборка

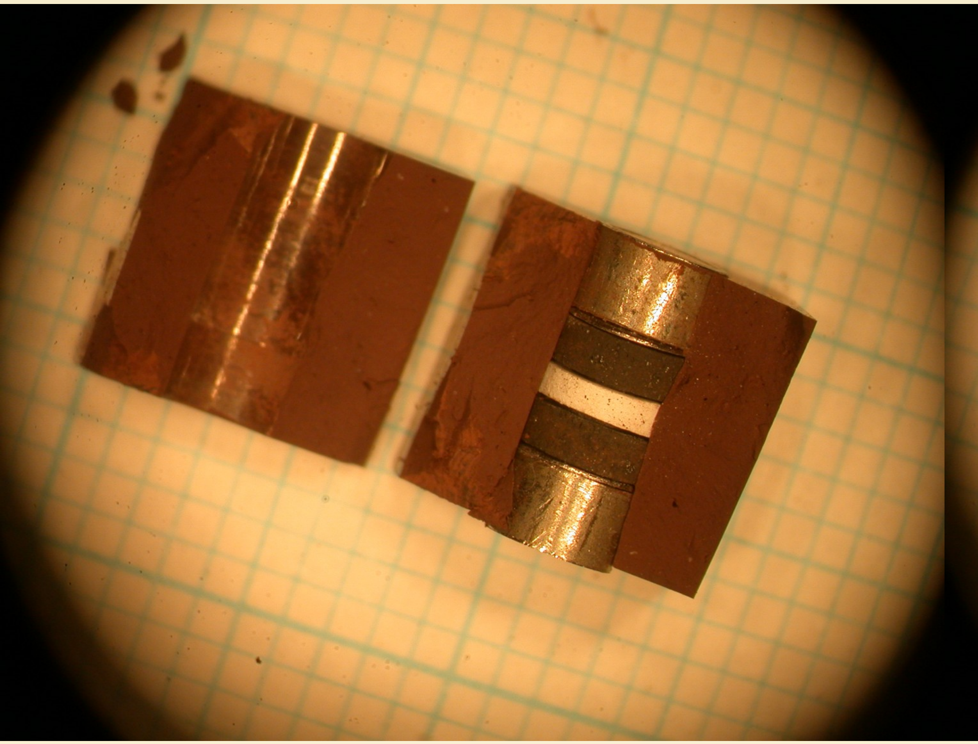

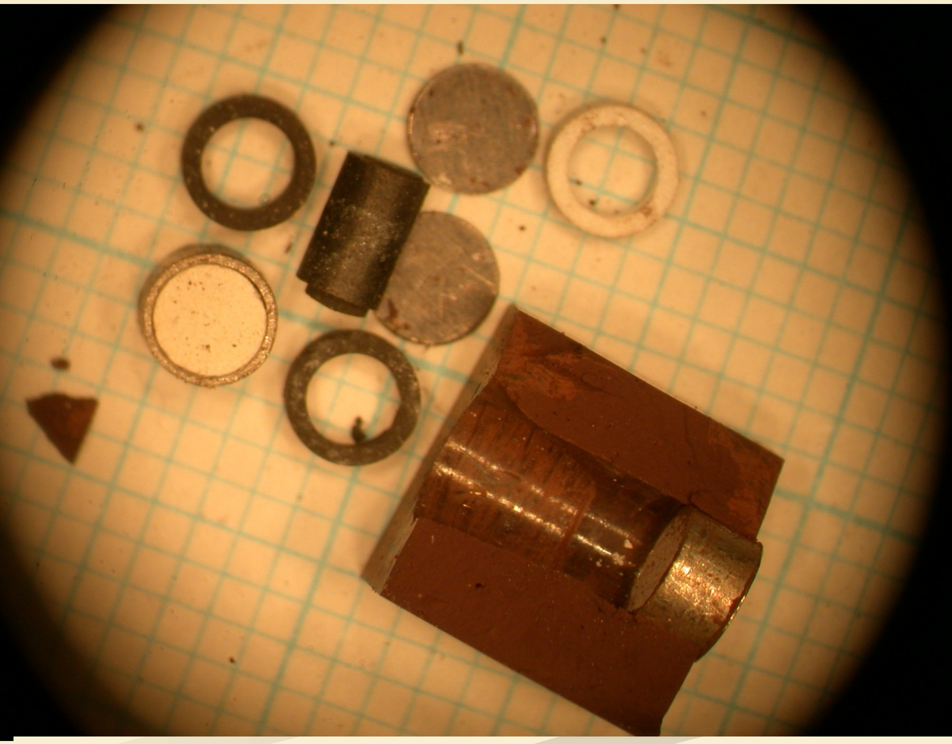

After 8 GPa and 1650C, 2 hours B2O3 new assembly with heat protectors

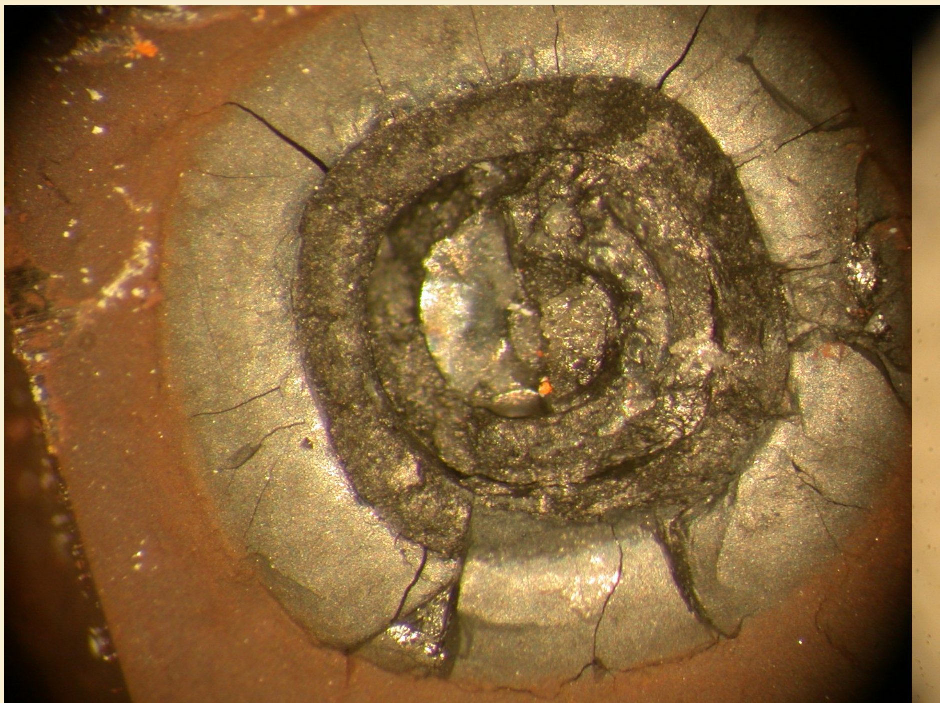

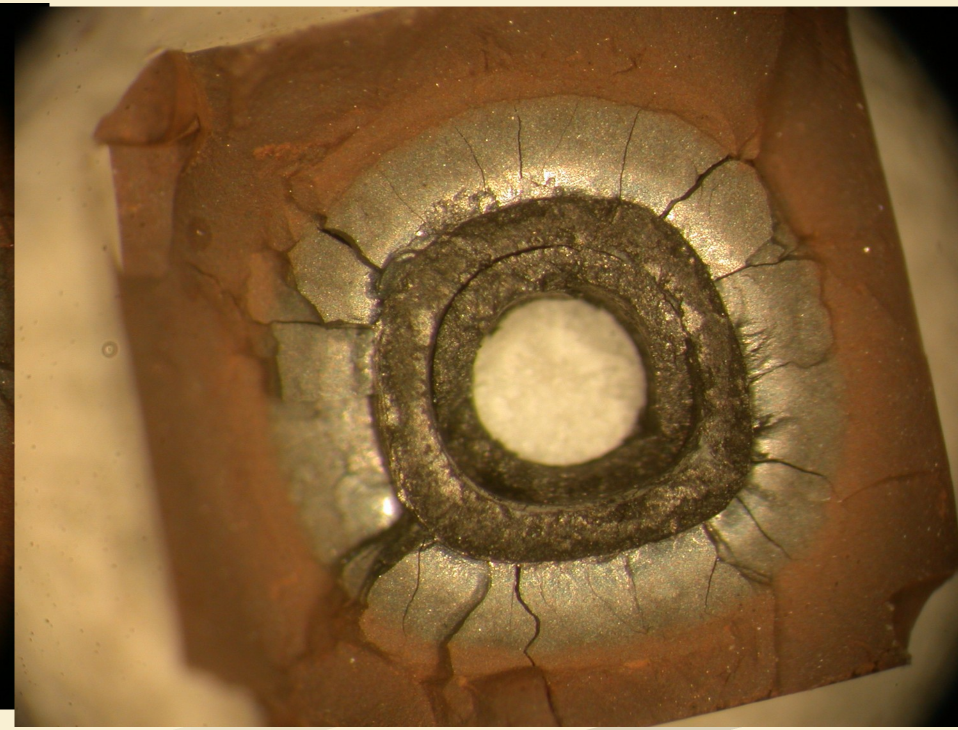

P.S.Вязкость в разных фазах расплавов

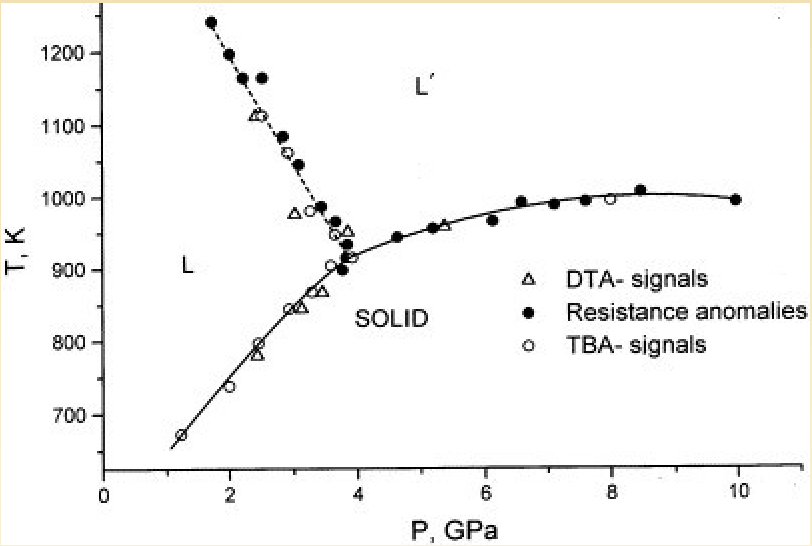

L'
L
SOLID
DTA- signals
Resistance anomalies
TBA- signals
T, K
P, GPa
1200
1100
1000
900
800
700
0
2
4
6
8
10

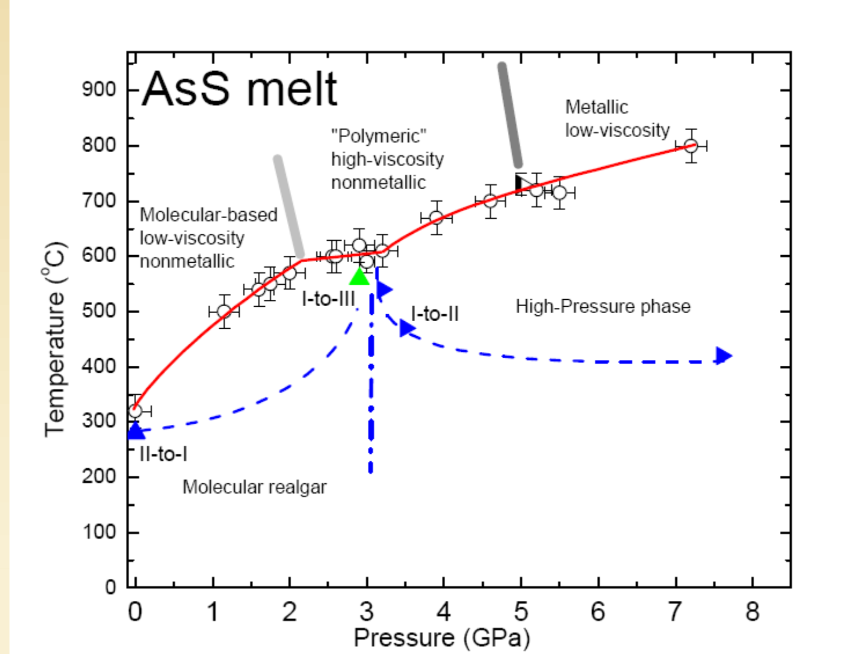

AsS melt
Metallic
low-viscosity
"Polymeric"
high-viscosity
nonmetallic
Molecular-based
low-viscosity
nonmetallic
I-to-III
I-to-II
High-Pressure phase
II-to-I
Molecular realgar
Temperature (°C)
Pressure (GPa)

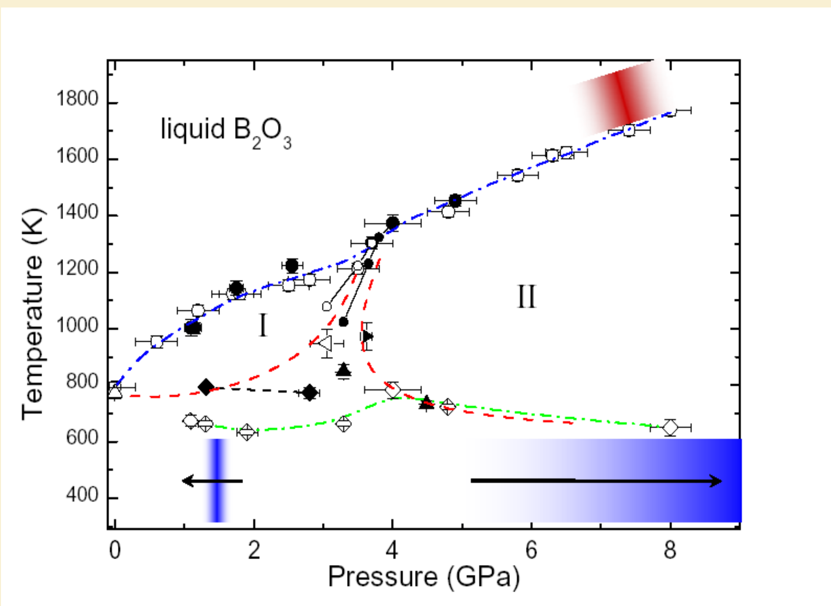

liquid B_2O_3
I
II
Temperature (K)
Pressure (GPa)

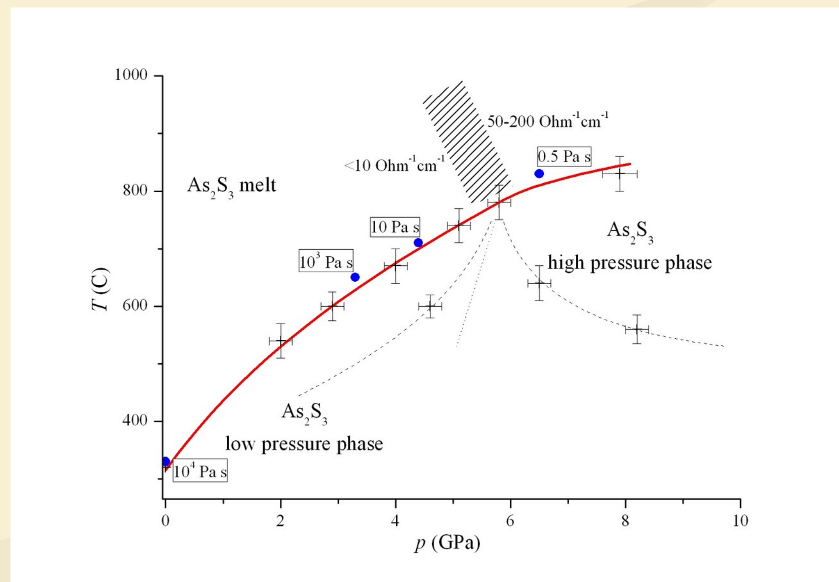

50-200 Ohm^{-1}cm^{-1}
<10 Ohm^{-1}cm^{-1}
0.5 Pa s
10 Pa s
10^3 Pa s
10^4 Pa s
As_2S_3 melt
As_2S_3
high pressure phase
As_2S_3
low pressure phase
T (C)
p (GPa)

Вязкость расплавов

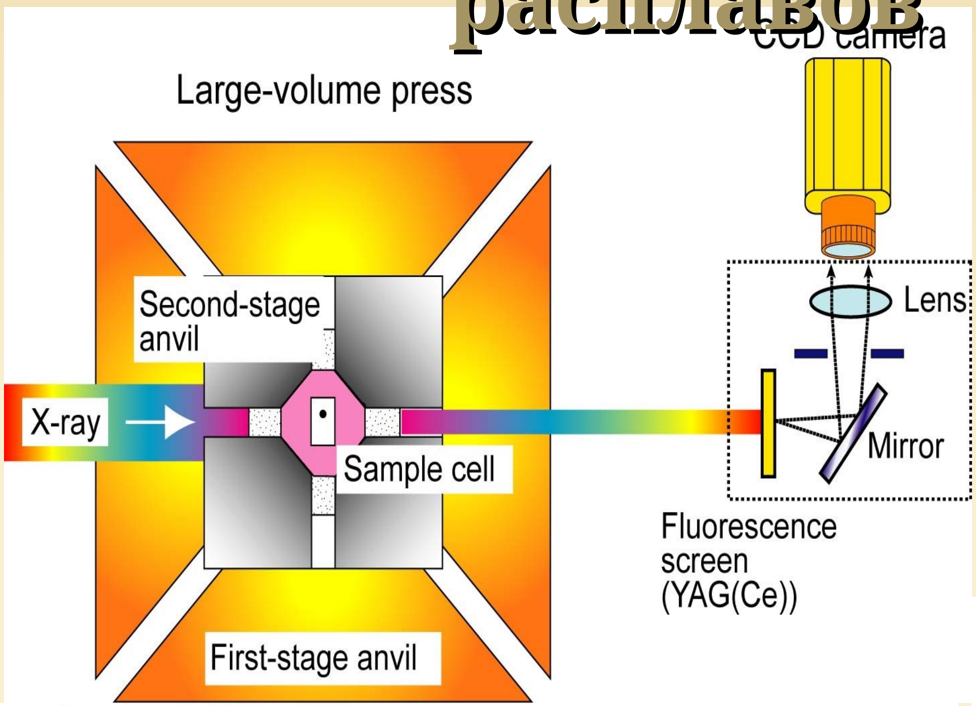

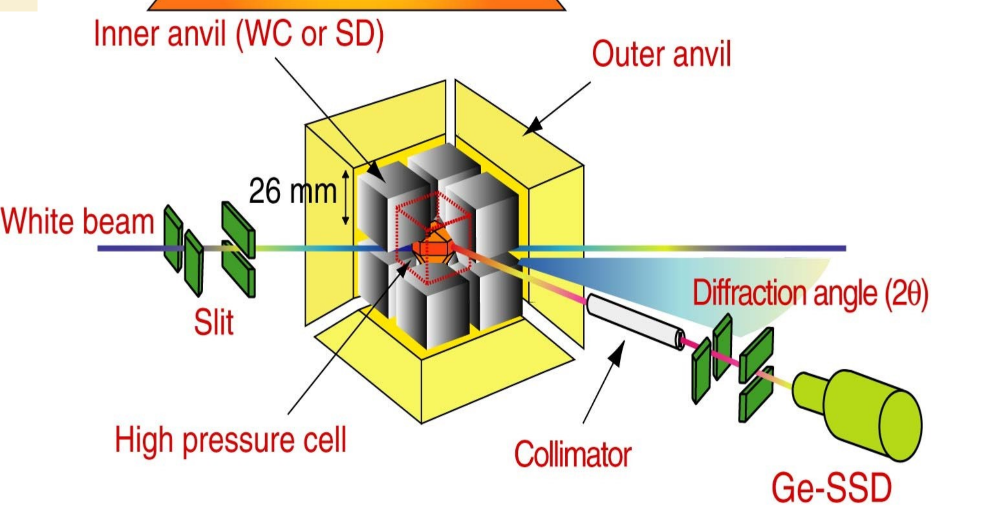

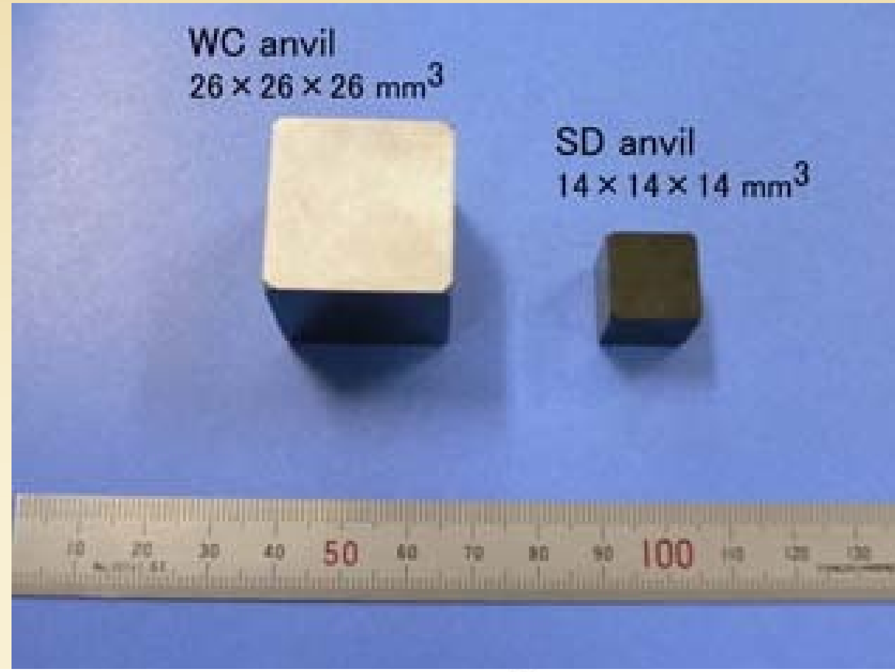

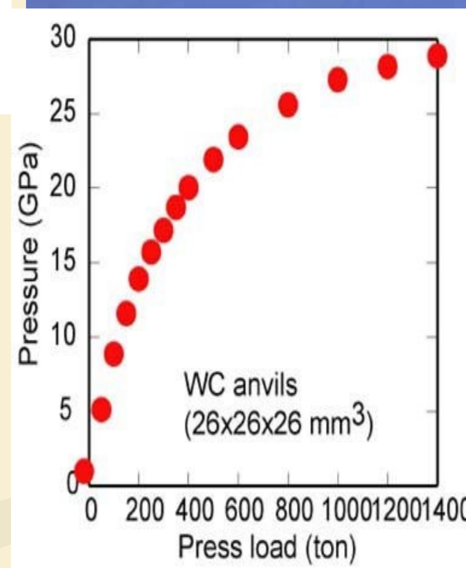

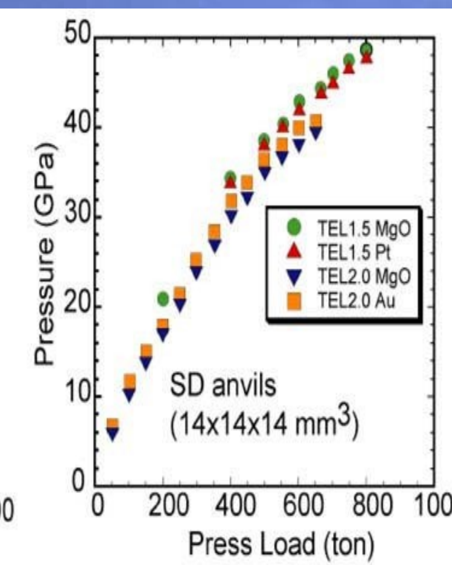

Radiography

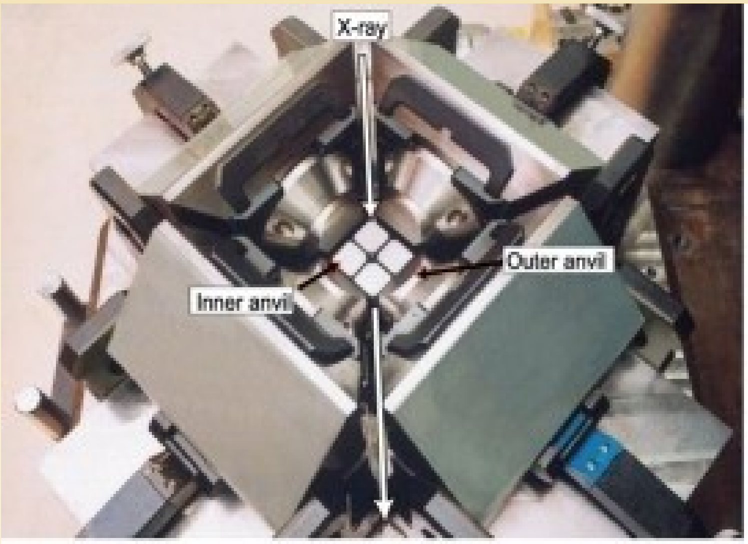

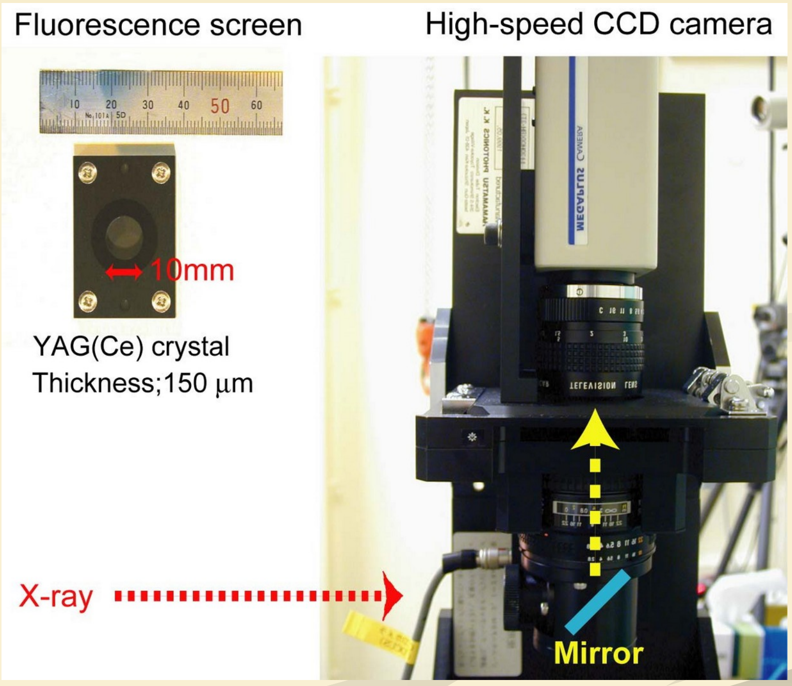

B2O3

Assembly preparation B2O3

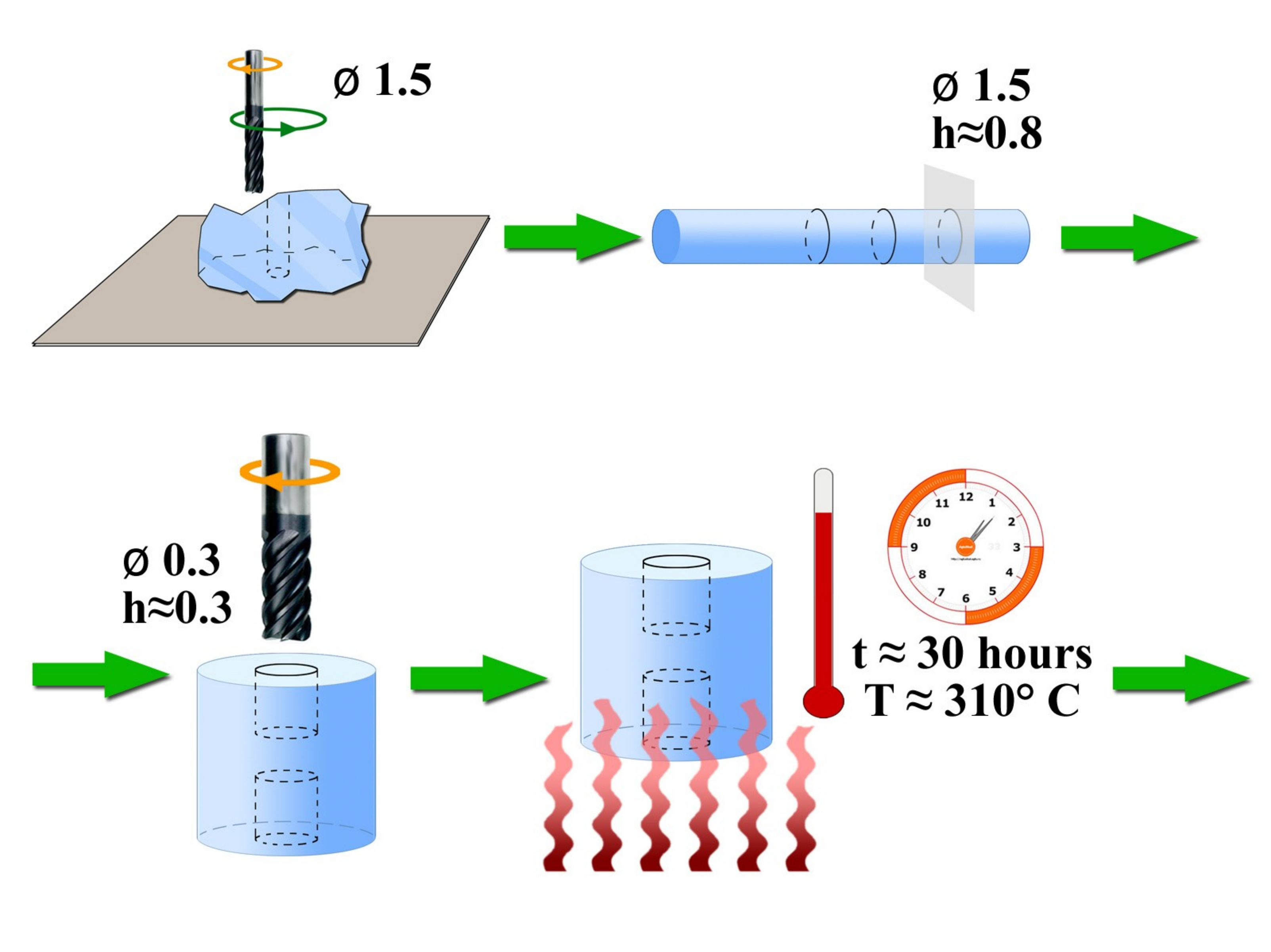

Assembly preparation B2O3

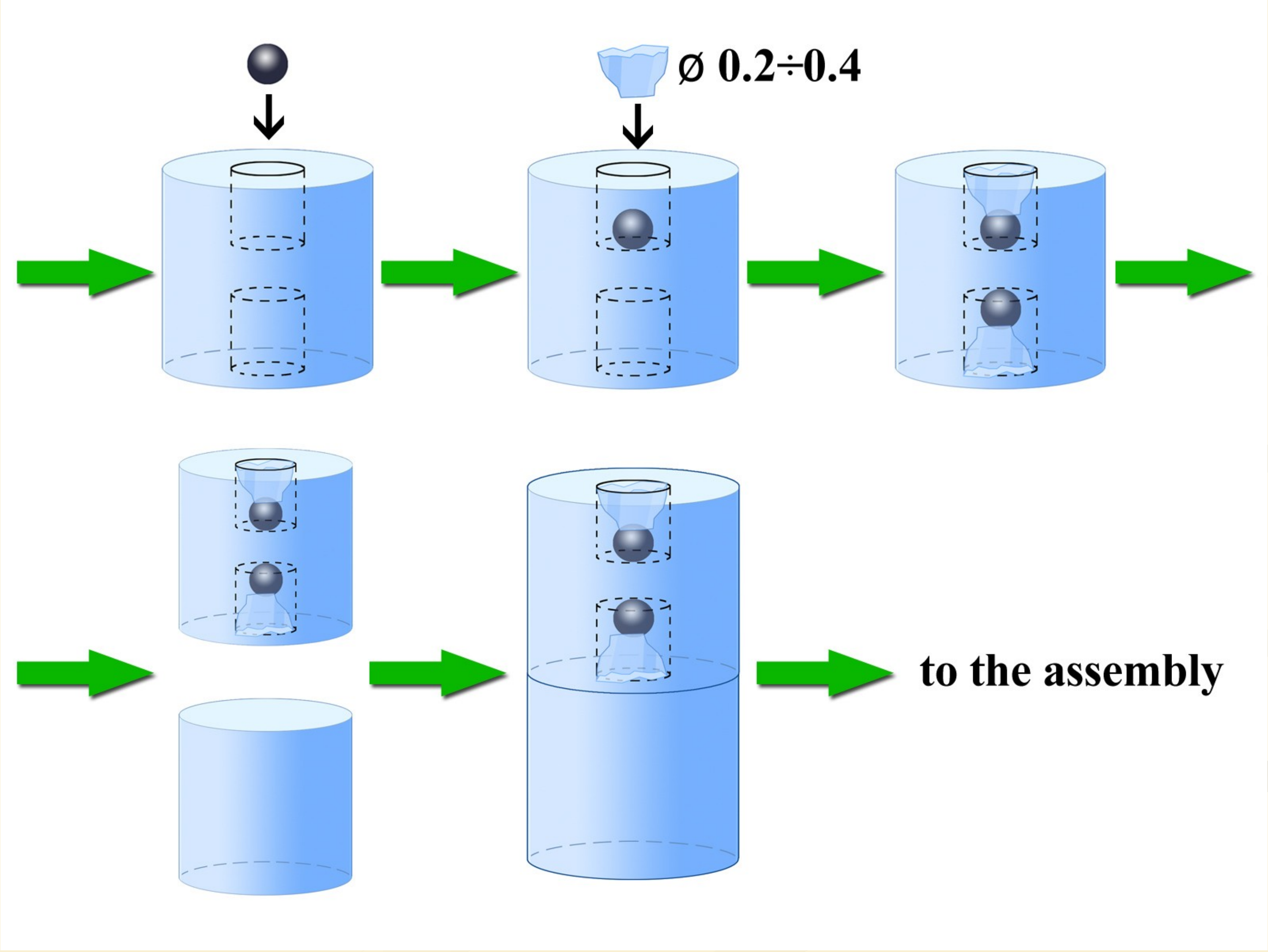

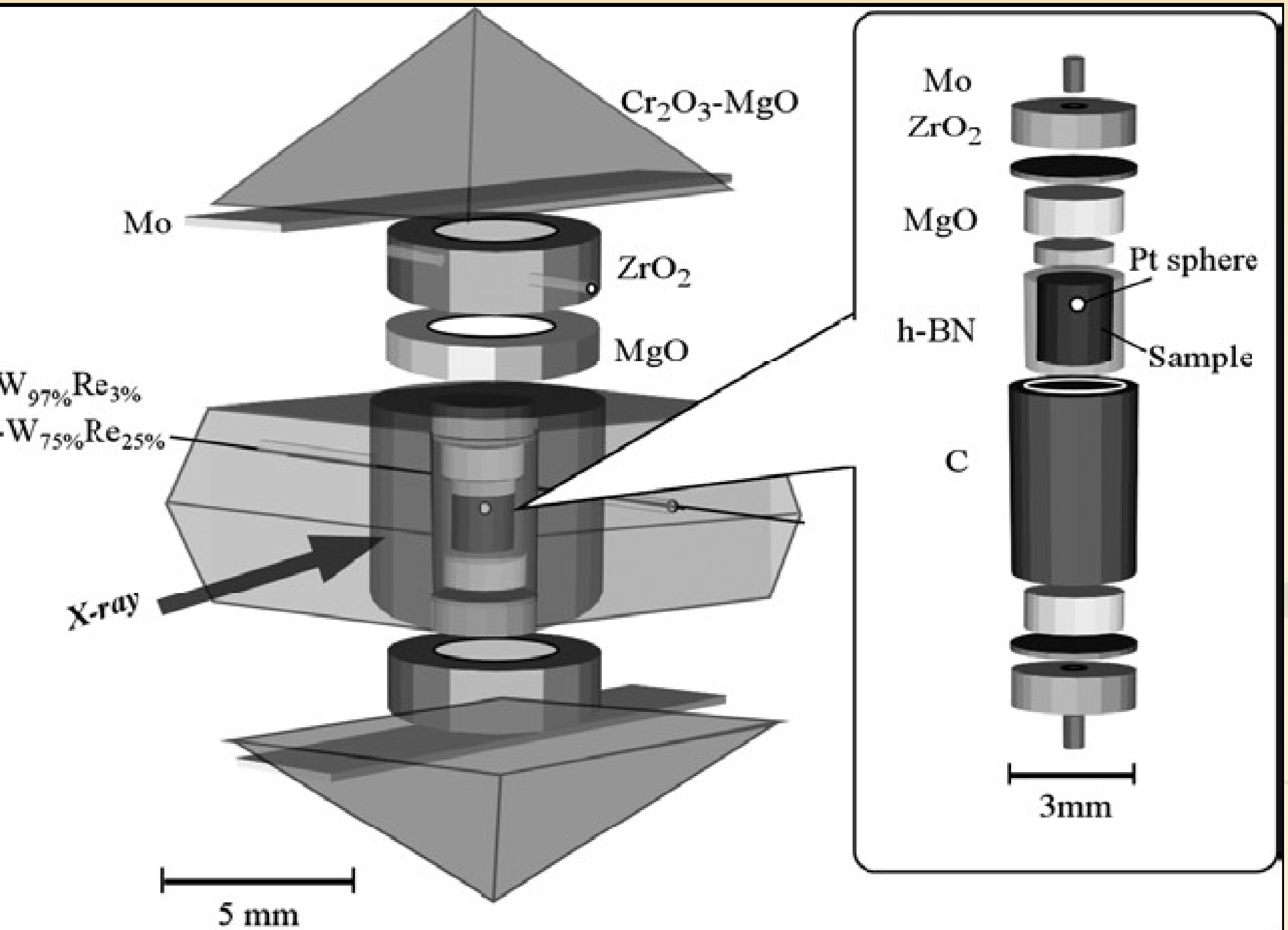
Cr_2O_3-MgO
Mo
ZrO_2
MgO
$W_{97\%}Re_{3\%}$
-$W_{75\%}Re_{25\%}$
X-ray
5 mm
Mo
ZrO_2
MgO
Pt sphere
h-BN
Sample
C
3mm

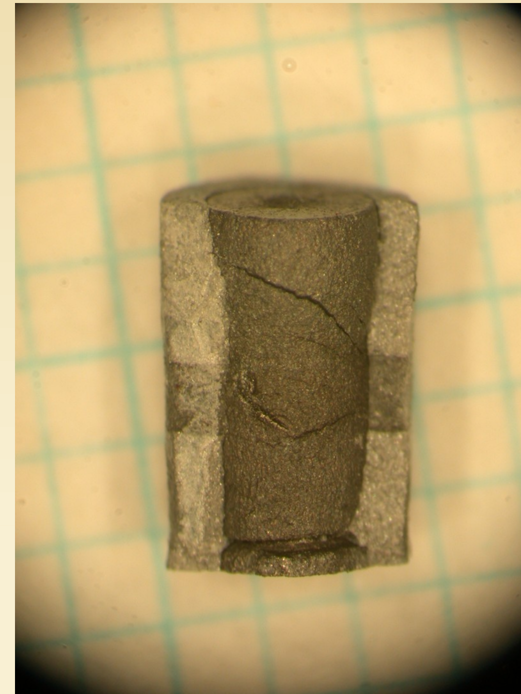

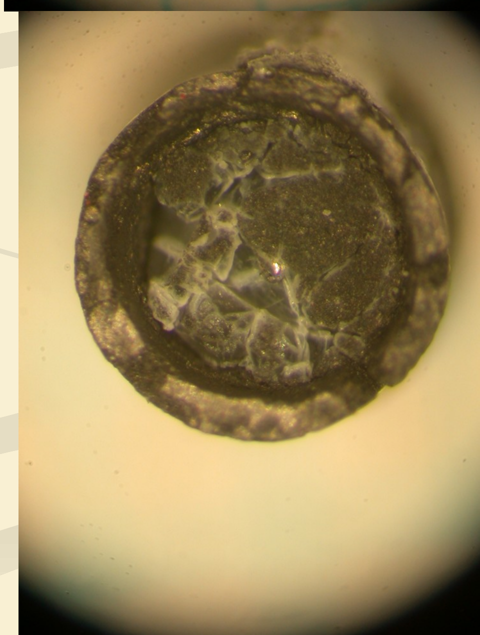

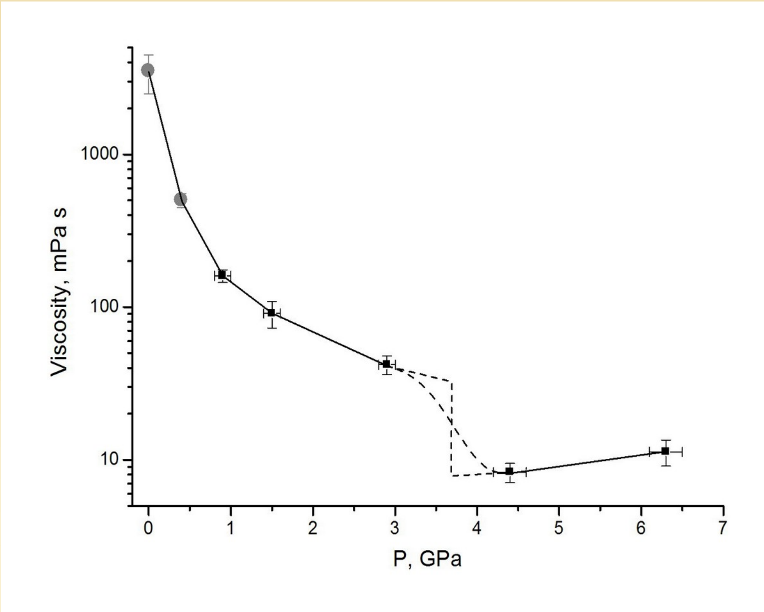

Viscosity, mPa s
1000
100
10
0
1
2
3
4
5
6
7
P, GPa

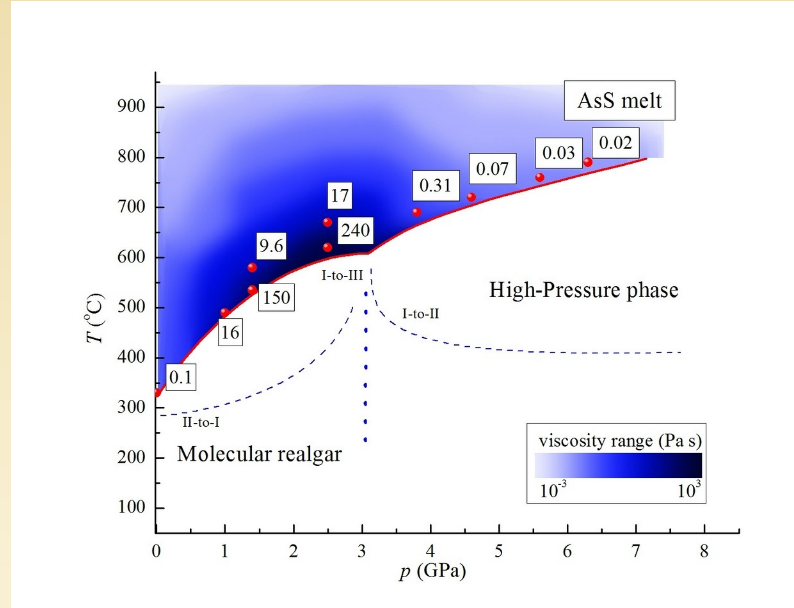

AsS melt
900
800
700
600
500
400
300
200
100
T (°C)
0.02
0.03
0.07
0.31
17
240
9.6
150
16
0.1
I-to-III
I-to-II
II-to-I
High-Pressure phase
Molecular realgar
viscosity range (Pa s)
10^-3
10^3
0
1
2
3
4
5
6
7
8
p (GPa)

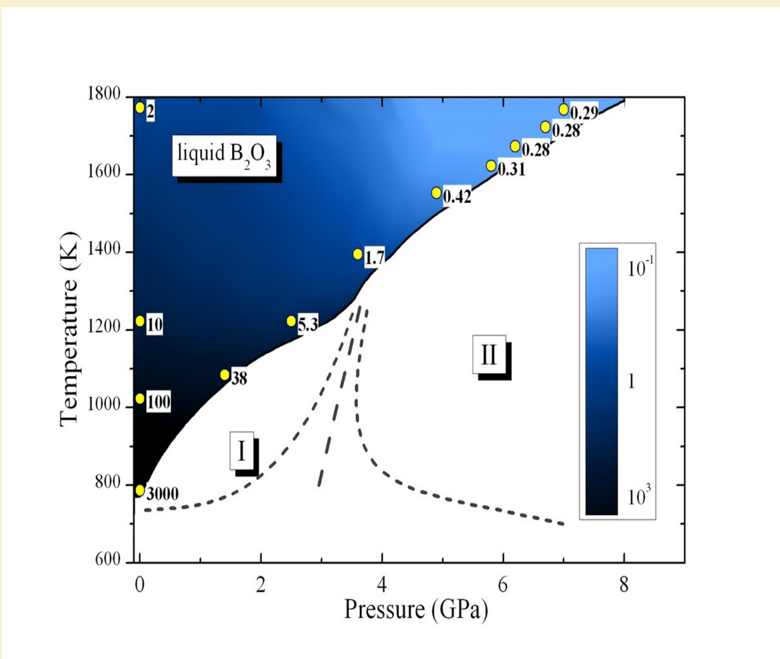

1800
1600
1400
1200
1000
800
600
Temperature (K)
2
liquid B2O3
0.29
0.28
0.28
0.31
0.42
1.7
5.3
10
38
100
3000
I
II
10^-1
1
10^3
0
2
4
6
8
Pressure (GPa)

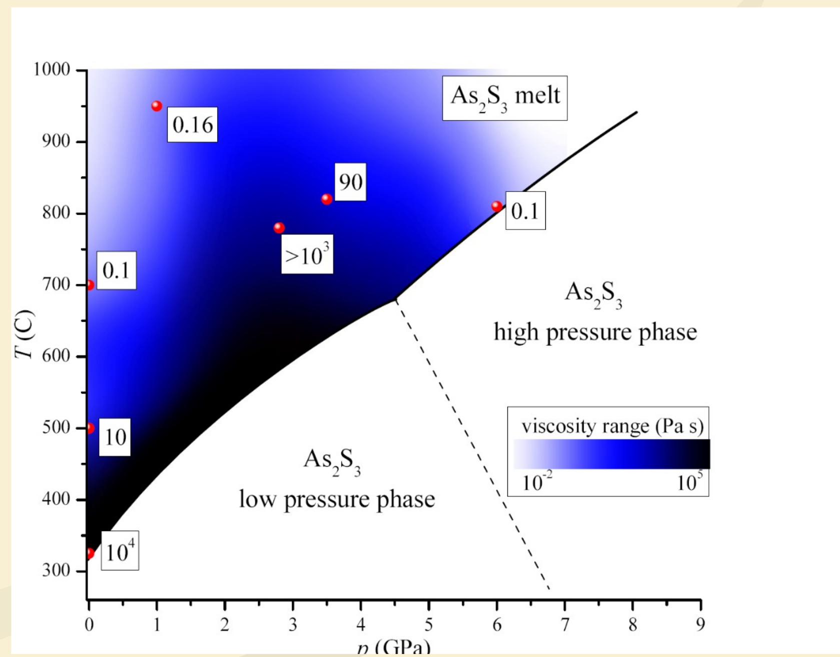

1000
900
800
700
600
500
400
300
T (C)
As2S3 melt
0.16
90
>10^3
0.1
0.1
10
10^4
As2S3
high pressure phase
As2S3
low pressure phase
viscosity range (Pa s)
10^-2
10^5
0
1
2
3
4
5
6
7
8
9
p (GPa)

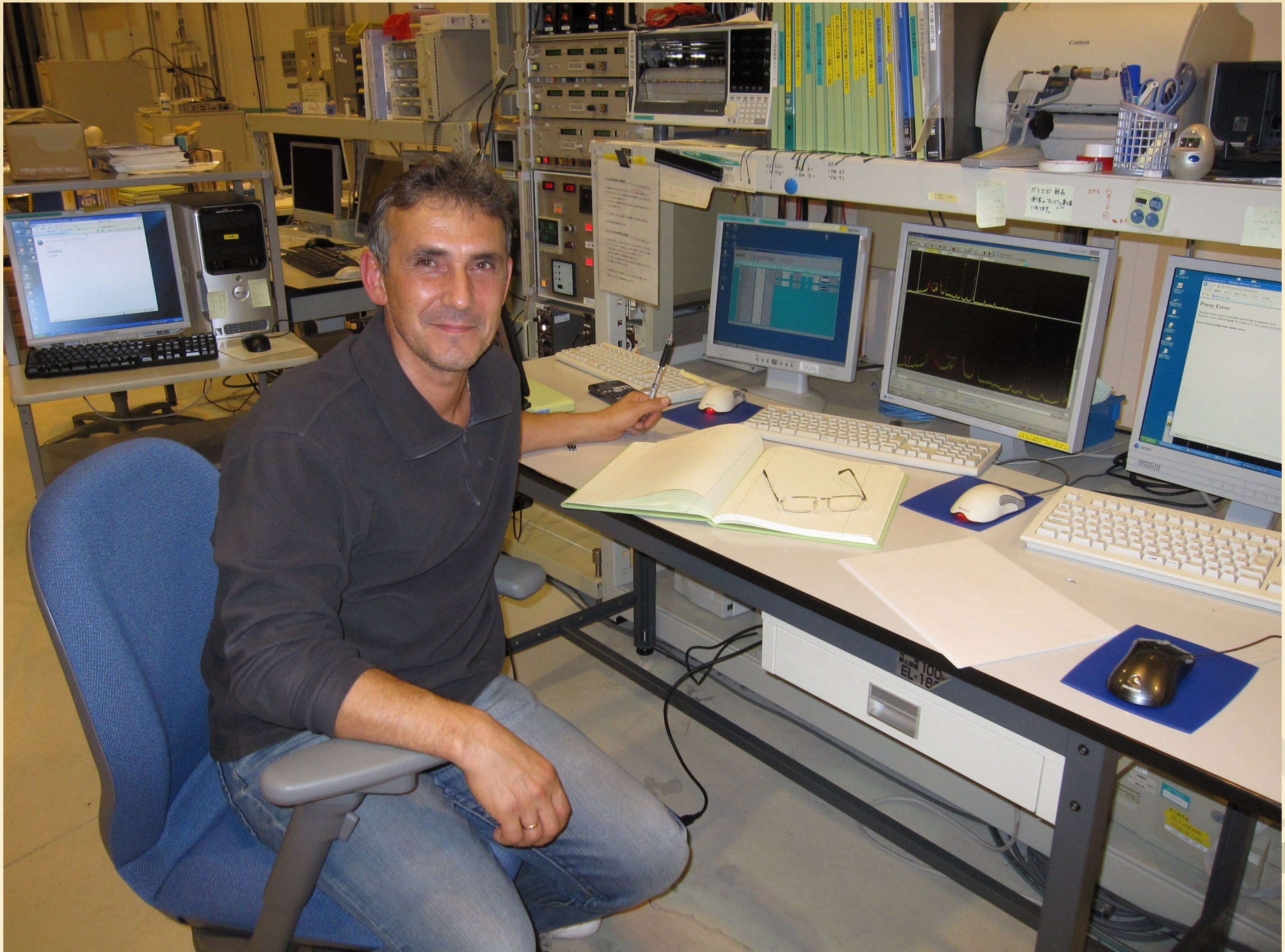
Proxy Error


5-56


使用室
自動扉制御盤
KAWASAKI
BL14B1

After 18 shifts

- Спасибо за внимание

  (а сейчас – кино)